An indicator-based problem reduction scheme for coupled reactive transport models

Brubeck Lee Freeman
Peter John Cleall
Anthony Duncan Jefferson*

Cardiff University, School of Engineering, Queen's Buildings, The Parade CF24 3AA, UK

www.cardiff.ac.uk

*jeffersonad@cardiff.ac.uk

Abstract

A number of effective models have been developed for simulating chemical transport in porous media; however, when a reactive chemical problem comprises multiple species within a substantial domain for a long period of time, the computational cost can become prohibitively expensive. This issue is addressed here by proposing a new numerical procedure to reduce the number of transport equations to be solved. This new problem reduction scheme (PRS) uses a predictor-corrector approach, which 'predicts' the transport of a set of non-indicator species using results from a set of indicator species before 'correcting' the non-indicator concentrations using a mass balance error measure. The full chemical transport model is described along with an experimental validation. The PRS scheme is then presented together with an investigation, based on a 16 species reactive advective-diffusion problem, which determines the range of applicability of different orders of PRS. The results of a further study are presented in which a set of PRS simulations are compared with those from full model predictions. The application of the scheme to the intermediate-sized problems considered in the present study showed reductions of up to 82 % in CPU time with good levels of accuracy maintained.

Keywords:

Problem Size Reduction, Reactive Transport, Coupled Models, Finite Element

Nomenclature

c	*Chemical concentration [kg/kg]*
$\overline{\mathbf{C}}$	*Global storage matrix*
$D^{\pi}/\mathbf{D}^{\pi}$	*Diffusion coefficient/tensor for phase π [m²/s]*
F	*Faraday constant [C/mol]*
$\overline{\mathbf{F}}$	*Global RHS vector*
$\mathbf{g}$	*Gravity vector [m/s²]*
$\mathbf{J}_{\pi}$	*Flux of phase π*
$K_i/\mathbf{K}_i$	*Permeability coefficient/tensor of Type i [m²/-]*
$\overline{\mathbf{K}}$	*Global flux matrix*
k_d, k_a	*Desorption and Adsorption Rate Parameters*
m_{π}	*Mass of phase π*
n	*Porosity*
$\mathbf{N}$	*Shape function vector*
ne	*Number of elements*
n_{ind}	*Number of indicator species*
np	*Number of precipitates/sorbed masses*
ns	*Number of species*
$\mathbf{n}$	*Unit normal vector to boundary*
P_C	*Capillary pressure [Pa]*
q_{π}	*Imposed flux of phase π*
r	*Reaction rate [1/s]*
R	*Ideal gas constant [J/K*kmol]*
RH	*Relative humidity*
S_{π}	*Degree of saturation of phase π*
t	*Time [s]*
T	*Temperature [K]*
$\mathbf{v}_{\pi}$	*Velocity of phase π [m/s]*
z	*Charge of chemical species*

Greek Letters

α_T, α_L	*Transverse and longitudinal dispersivities*
β_c	*Moisture transfer coefficient [m/s]*
γ_c	*Chemical transfer coefficient [kg/m² s]*
δ_{kj}	*Kronecker delta*
ε	*Dielectric permittivity [F/m]*
μ, λ	*Rate parameters*
μ_w	*Dynamic viscosity [Pa*s]*
ρ_π	*Density of phase π [kg/m³]*
$\overline{\rho_\pi}$	*Phase averaged density of phase π*
τ	*Characteristic time [s]*
$\boldsymbol{\varphi}$	*Vector of residuals*
ψ	*Local electric field*
Γ_π	*Boundary of domain*
$\boldsymbol{\Phi}$	*Vector of primary variables*
Ω	*Total domain*
Ω^e	*Element domain*

Subscripts/Superscripts

0	*Initial*	ind/jnd	*Indicator*
b	*Boundary*	k	*Iteration number*
c	*Cauchy*	mol	*Molecular*
C	*Capillary*	mv	*Moisture vapour*
d	*Dispersive*	p	*Precipitated/Sorbed*
D	*Dirichlet*	r	*Reference*
e	*Element*	rw	*Relative water*
env	*Environment*	s	*Solid*
es	*Electrostatic double layer*	SIS	*Source influence solution*
g	*Gas*	τ	*Tortuosity*
gr	*Gradient*	u/l	*Upper/Lower*
i	*Chemical species i*	v	*Vapour*
in	*Intrinsic*	W	*Water*

1 Introduction

The prediction of chemical solute transport behaviour in porous media is of great importance in a wide range of engineering applications. To this end, a significant number of numerical transport models have been developed. Typically, these are coupled models which consider advection and hydrodynamic dispersion, the latter of which comprises both mechanical dispersion and self-diffusion[1] of the chemical species coupled with heat flow, and often, the mechanical behaviour of the medium. In addition to these flow and deformation processes, the solute can also be considered to be either reactive or non-reactive depending on the nature of the problem considered.

The application of these models has varied considerably, with many studies concentrating on geochemical problems such as modelling groundwater systems,[2-6] assessing the performance of engineered barriers,[7-11] or attenuation of mine water tailings.[12-14] Application of these models to cementitious materials has most often investigated the ingress of chloride ions[15-18] or calcium leaching;[19,20] however, recently these models have also been used for the investigation of self-healing concrete.[21,22]

One of the major disadvantages of these models is that they can become computationally expensive when the chemical system becomes relatively large. Cleall et al.[23] suggest that the magnitude of a problem is governed by three main aspects; the domain size, timescale and the complexity of the analysis, which includes the number of variables, the degree of coupling between them, the number of processes considered and the degree of nonlinearity of the system. The degree of nonlinearity depends on the underlying physical processes; for example, the system will be highly nonlinear if the

reactions are sensitive to small changes in concentration, or the permeability of the porous medium is sensitive to the degree of saturation. To deal with this issue, several techniques have been proposed to improve the computational efficiency of the associated solution process; including, 'operator splitting' techniques and reformulation of the coupled system. Operator splitting divides or 'splits' a time step into a transport calculation and a reaction calculation, to be solved sequentially, with many models iterating between the two. This is an approximation of the time integral of the governing equation,[24] which therefore changes the numerical framework from a global implicit approach (GIA) to a sequential iterative or sequential non-iterative approach (SIA/SNIA). Such calculation splitting methods have been found to reduce the computational cost[25] and have been used by many authors.[2-4,8-11] A disadvantage of the SNIA approach is its propensity to introduce splitting errors (for example mass balance errors), whilst the SIA tends to require prohibitively small time steps and a relatively large number of iterations to achieve convergence.[26,27] Consequentially, these operator splitting approaches have been found to increase computational demand for certain 'chemically difficult' cases (for example, cases with high kinetic reaction rates).[27,28]

A number of authors have taken an alternative approach, concentrating instead on improving the efficiency of GIAs. Most studies have focussed on reformulating the system by decoupling a number of the partial differential equations (PDEs) and eliminating certain local (spatially invariant) equations, including both ordinary differential equations (ODEs) and algebraic equations (AEs).[26,27,29-31] A common assumption used in such formulations is that all chemical species have the same diffusion coefficient.[26,27] This has been justified by the fact that predicted responses are relatively insensitive to differences in diffusion constants because mechanical dispersion is normally the dominant transport mechanism.[27] An alternative view was expressed by Thomas et al.[10] who suggested that this assumption is not valid for some chemical systems. The presence of minerals whose concentrations can reach zero may also cause issues when such schemes are used,[26] although Kräutle and Knabner[26] have introduced a moving boundary condition and a complimentary function to alleviate these difficulties.

The reduction in computational demand that can be achieved by the operator-splitting and reformulation approaches described above is often limited by the chemistry of a problem; for example, only limited reductions are possible when a large number of kinetic reactions with high reaction rates are considered. To address this issue, an indicator-based multi-order problem reduction scheme is proposed, which allows a greater reduction in problem size that is independent of the nature of reactions, and which explicitly considers species-dependent diffusion coefficients. The scheme works by decoupling a number of the nonlinear PDEs from the global system of equations. In this new Problem Reduction Scheme (PRS), a small number of indicator species (≤3) are selected for full computation and then, on a step-wise basis, the response of other species is inferred from these indicators using a predictor-corrector approach. The reduction in computational demand is achieved through the reduction in size of the nonlinear global system of equations and by the replacement of nonlinear PDEs with step-wise predictor-corrector computations for non-indicator species. Three different orders of the PRS are considered, each applicable to different chemical systems. The new PRS is presented along with a study to establish the range of applicability of each order considered. This is followed by a set of validation examples in which the reactive transport of chemical species through mortar and concrete specimens is simulated.

2 Theoretical Formulation

2.1 Mathematical model

The theoretical model is based on the approach of Gawin et al.[32] The porous medium is assumed to be composed of three main phases namely; solid skeleton, liquid moisture and gas, the latter of which consists of dry air and moisture vapour. It is also assumed that dissolved chemical species are present in the liquid moisture phase and that precipitation can occur. Following the approach of Chitez and Jefferson,[33] the combined gas pressure of dry air and moisture vapour is assumed to remain constant at atmospheric pressure but that the moisture vapour may diffuse through the gas phase.

The primary variables considered here are the capillary pressure (P_C), and chemical concentration (c_i) of each species. The advantages of using capillary pressure as the primary moisture variable have been discussed by Gawin et al.[32] These include the fact that it is convenient for coupling moisture flow to mechanical behaviour, due to the direct relationship that exists between the pressure and the components of stress, and that it provides a physically meaningful driving force for moisture flow.

Macroscopic balance equations, as derived from the volume averaging theorem and hybrid mixture theory,[34] are presented in the following sections. Heat transport is included in the model, governed by the enthalpy balance equation; however, the problems considered here are isothermal and so this part of the model has not been used in the present study.

2.2 Governing Equations

2.2.1 Moisture transport

Transport in the porous medium is described using mass balance equations for liquid moisture, moisture vapour and chemical species. Defining the domain $\Omega \in \mathbb{R}^d$ with boundary Γ, and noting that the time interval considered is given as $t \in [t_0, T]$, the mass balance of the liquid moisture and moisture vapour can be written as:

$$\partial_t(nS_w\rho_w) + \boldsymbol{\nabla} \cdot (nS_w\rho_w\mathbf{v}_w) + \partial_t(m_v) = 0 \qquad \forall\, \mathbf{x} \in \Omega \qquad (1)$$

$$\partial_t\left(nS_g\rho_v\right) + \boldsymbol{\nabla} \cdot \mathbf{J}_\mathrm{v} - \partial_t(m_v) = 0 \qquad \forall\, \mathbf{x} \in \Omega \qquad (2)$$

Summing these together gives the total mass balance for moisture:

$$\partial_t(nS_w\rho_w) + \partial_t\left(nS_g\rho_v\right) + \boldsymbol{\nabla} \cdot (nS_w\rho_w\mathbf{v}_w) + \boldsymbol{\nabla} \cdot \mathbf{J}_v = 0 \qquad \forall\, \mathbf{x} \in \Omega \qquad (3)$$

where n denotes the porosity, S_w is the degree of liquid moisture saturation and ρ_w is the liquid density, S_g is the degree of gas saturation and ρ_v the moisture vapour density. ∂_t denotes a time derivative, $\mathbf{v}_w$ is the liquid moisture velocity, $\partial_t(m_v)$ is the rate of moisture transfer from liquid to vapour and $\mathbf{J}_v$is the moisture vapour diffusion described here by Fick's law:[32]

$$\mathbf{J}_v = -\rho_g \mathbf{D}^{\mathbf{mv}} \boldsymbol{\nabla}\left(\frac{\rho_v}{\rho_g}\right) \qquad (4)$$

where ρ_g is the gas density and $\mathbf{D}^{\mathbf{mv}}$ is the moisture vapour diffusivity tensor given by:[22]

$$D_{i,j}^{mv} = \begin{cases} n(1-S_w)^{A_v} f_v D^{v0} \left(\frac{T}{T_r}\right)^{B_v} \frac{P_{atm}}{P_g} & \forall\, i = j \\ 0 & \forall\, i \neq j \end{cases} \quad (5)$$

where A_v=1, B_v=1.667 and f_v=0.01. D^{v0}=2.47x10^{-5} m^2/s is the moisture vapour diffusion coefficient in air, T_r=273 K is the reference temperature, and P_g and P_{atm} denote the gas pressure and atmospheric pressure respectively.

The flow of the liquid moisture through the medium can be described by Darcy's law:[32]

$$nS_w \mathbf{v}_w = \frac{\mathbf{K}_{\text{in}} K_{rw}}{\mu_w} (\boldsymbol{\nabla} P_C + \rho_w \mathbf{g}) \quad (6)$$

where $\mathbf{K}_{\text{in}}$ is the intrinsic permeability tensor of the medium, μ_w is the viscosity of the fluid and K_{rw} is the relative permeability of the moisture phase given by:[8]

$$K_{rw} = S_w^{A_w} \quad (7)$$

where A_w=4 in the present work.

The remaining constitutive relationships used in the moisture transport component of the model are given in Appendix A.

2.2.2 Chemical transport

The mass balance of a dissolved chemical species, i, can be written as:

$$\partial_t (nS_w \rho_w c_i) + \boldsymbol{\nabla} \cdot (nS_w \rho_w c_i \mathbf{v}_w) + \boldsymbol{\nabla} \cdot \mathbf{J}_d^i - n\rho_p \partial_t \left(S_p\right)_i = 0 \qquad \forall\, \mathbf{x} \in \Omega \quad (8)$$

where the final term on the left hand side is the source/sink term due to chemical reactions, S_p is the degree of saturation of precipitated or sorbed material, ρ_p is the mass of the precipitated or sorbed material and $\mathbf{J}_d^i$ is the dispersive flux given by the Poisson Nernst Planck equations, which can be written as follows[35], where the first term on the right hand side of eq. (9) represents mechanical dispersion and the remaining r.h.s. terms account for diffusion:

$$\mathbf{J}_d^i = -\rho_w \mathbf{D}_i^d \cdot \boldsymbol{\nabla} c_i - nS_w \rho_w D_i^{mol} (\boldsymbol{\nabla} c_i + \frac{z_i F}{RT} c_i \boldsymbol{\nabla} \psi) \quad (9)$$

$$\varepsilon \nabla^2 \cdot \psi + F(\textstyle\sum_{i=1}^{ns} z_i c_i + \rho) = 0 \quad (10)$$

D_i^{mol} is the coefficient of molecular diffusion, z is the charge of an ion, ε is the dielectric permittivity, ρ is the charge density, F is Faraday's constant and ψ is the electrical potential. $\mathbf{D}_i^d$ is the mechanical dispersion tensor, defined below in equation 14. The second term in the bracket in eq. (9) represents dispersion due to the local electric field ψ which can be calculated from eq. (10). It can be noted that the first term in eq. (10) is negligible,[35,36] as is the charge density ρ, thus eq. (10) reduces to the following charge neutrality condition: [10,35-37]

$$\textstyle\sum_{i=1}^{ns} z_i c_i = 0 \quad (11)$$

and, since the pore solution is initially charge neutral, this condition is ensured through the no electrical current condition:[10,36,37]

$$\sum_{i=1}^{ns} z_i \mathbf{J}_i = 0 \tag{12}$$

where $\mathbf{J}_i = -nS_w\rho_w D_i^{mol}(\boldsymbol{\nabla} c_i + \frac{z_i F}{RT} c_i \boldsymbol{\nabla}\psi)$ is the diffusive flux of species i.

Equation (12) can be used to eliminate the electrical potential gradient giving the dispersive flux of species i as:

$$\mathbf{J}_d^i = -\rho_w \mathbf{D}_i^d \cdot \boldsymbol{\nabla} c_i - nS_w\rho_w D_i^{mol}\left(\boldsymbol{\nabla} c_i + z_i c_i \frac{\sum_{i=1}^{ns} z_i D_i^{mol} \boldsymbol{\nabla} c_i}{\sum_{i=1}^{ns} z_i^2 D_i^{mol} c_i}\right) \tag{13}$$

The hydrodynamic dispersion is the sum of the molecular diffusion and mechanical dispersion. The definition of hydrodynamic dispersion of Bear and Bachmat[1] is adopted here, where the mechanical dispersion tensor is given as:

$$D_i^d{}_{k,j} = \alpha_T |\mathbf{v}_w| \delta_{kj} + (\alpha_L - \alpha_T) \frac{v_w^k v_w^j}{|\mathbf{v}_w|} \tag{14}$$

where α_L and α_T are the longitudinal and transverse dispersivities respectively and δ_{kj} is the Kronecker delta ($\delta_{kj} = 1\ if k{=}j$ or $\delta_{kj} = 0\ if\ k{\neq}j$).

2.2.3 Chemical reactions

The chemical reactions considered here are all assumed to be non-equilibrium reactions, i.e. transport of the ions may be faster than the rate of reactions such that binding or precipitation is not instantaneous.[38] In addition, it is assumed that the rates of the reaction can be computed using a Freundlich type isotherm, as follows:[35]

$$\partial_t (S_p)_i = -\frac{(S_p - \mu c_i{}^{\lambda})}{\tau} \tag{15}$$

in which, μ and λ are rate parameters, and τ is a characteristic time that accounts for non-equilibrium behaviour. It can be noted that molar concentrations are used to calculate the reaction rates throughout.

2.3 Boundary conditions

In order to solve the system, both the initial conditions and boundary conditions (BC) are required. The initial conditions considered here define the values of all variables at time $t{=}t_0$ throughout the domain and on the boundary as follows:

$$P_C = P_C^0 \qquad c_i = c_i^0 \qquad \forall\, \mathbf{x} \in \Omega \tag{16}$$

The boundary conditions considered here are of the Cauchy type and Dirichlet type. The former are a combination of imposed fluxes (which in isolation describe Neumann boundary conditions)[32] and convective fluxes, which are a function of the difference in variables between the sample and the environment. Applied to the governing mass balance equations of moisture and of dissolved chemical species, the Cauchy boundary conditions describe the rate of mass transfer from the environment to the sample and are given as:

$$(nS_w\rho_w \mathbf{v}_w + \mathbf{J}_v) \cdot \mathbf{n} - q_v - q_w - \beta_c(\rho_v - \rho_v^{env}) \qquad \forall\, \mathbf{x} \in \Gamma_{c1} \tag{17}$$

$$\left(nS_w\rho_w c_i \mathbf{v}_w + \mathbf{J}_d^i\right) \cdot \mathbf{n} - q_c - \gamma_c(c_i - c_i^{env}) \qquad \forall\, \mathbf{x} \in \Gamma_{c2} \tag{18}$$

where q_w, q_v and q_c are the prescribed fluxes of the moisture, moisture vapour and chemical species respectively, and β_c and γ_c are the convective transfer coefficients of the moisture and chemical species respectively. $\mathbf{n}$ is the unit normal vector to the boundary.

The Dirichlet boundary conditions fix the value of the variable on the boundary and are given by:

$$P_c(t) = P_c^{\Gamma} \qquad \forall\, \mathbf{x} \in \Gamma_{D1} \tag{19}$$

$$c_i(t) = c_i^{\Gamma} \qquad \forall\, \mathbf{x} \in \Gamma_{D2} \tag{20}$$

3 Numerical Solution

In the present study, the governing equations (3 and 8) are discretised using the finite element method. The resulting variational problem, after the application of Gauss-Green divergence theorem, may be written as follows:

find $\mathbf{\Phi} \in U$, such that,

$$\int_\Omega \mathbf{W}\left(\partial_t(nS_w\rho_w) + \partial_t\left(nS_g\rho_v\right)\right)d\Omega - \int_\Omega \boldsymbol{\nabla}\mathbf{W}\cdot\left((nS_w\rho_w\mathbf{v}_w) + \mathbf{J}_v\right)d\Omega + \int_\Gamma \mathbf{W}\left(q_v + q_w + \beta_c(\rho_v - \rho_v^{env})\right)d\Gamma = 0 \tag{21}$$

$$\int_\Omega \mathbf{W}\left(nS_w\rho_w\partial_t(c_i) - n\rho_p\partial_t\left(S_p\right)_i\right)d\Omega - \int_\Omega \boldsymbol{\nabla}\mathbf{W}\cdot\left((nS_w\rho_w c_i\mathbf{v}_w) + \mathbf{J}_d^i\right)d\Omega + \int_\Gamma \mathbf{W}\left(q_c + \gamma_c(c_i - c_i^{env})\right)d\Gamma = 0 \tag{22}$$

where $\mathbf{\Phi} = [\overline{\mathbf{P}_c} \quad \overline{\mathbf{c}_i} \quad \dots \quad \overline{\mathbf{c}_{ns}}]$ is the vector of primary variables, and the space for the trial functions is defined as $U = \left\{\mathbf{u} \in H^1(\Omega) \;\middle|\; \mathbf{u}(\mathbf{x}) = \mathbf{\Phi}^{\Gamma} \quad \forall \mathbf{x} \in \Gamma_D\right\}$.

In this study, the continuous Galerkin weighted residual method[32] is employed such that the weight functions (**W**) are chosen to be equal to the shape functions (**N**), with the primary variables being the capillary pressure and the species' concentrations. The resulting system of discretised equations is as follows:

$$\begin{bmatrix} \overline{\mathbf{K}_{11}} & \overline{\mathbf{K}_{1i}} & \dots & \overline{\mathbf{K}_{1ns}} \\ \overline{\mathbf{K}_{i1}} & \overline{\mathbf{K}_{ii}} & \dots & \mathbf{0} \\ \vdots & \vdots & \ddots & \mathbf{0} \\ \overline{\mathbf{K}_{nsi}} & \mathbf{0} & \mathbf{0} & \overline{\mathbf{K}_{nsns}} \end{bmatrix} \begin{bmatrix} \overline{\mathbf{P}_c} \\ \overline{\mathbf{c}_i} \\ \vdots \\ \overline{\mathbf{c}_{ns}} \end{bmatrix} + \begin{bmatrix} \overline{\mathbf{C}_{11}} & \overline{\mathbf{C}_{1i}} & \dots & \overline{\mathbf{C}_{1ns}} \\ \overline{\mathbf{C}_{i1}} & \overline{\mathbf{C}_{ii}} & \dots & \mathbf{0} \\ \vdots & \vdots & \ddots & \mathbf{0} \\ \overline{\mathbf{C}_{nsi}} & \mathbf{0} & \mathbf{0} & \overline{\mathbf{C}_{nsns}} \end{bmatrix} \begin{bmatrix} \dot{\overline{\mathbf{P}_c}} \\ \dot{\overline{\mathbf{c}_i}} \\ \vdots \\ \dot{\overline{\mathbf{c}_{ns}}} \end{bmatrix} = \begin{bmatrix} \overline{\mathbf{F}_1} \\ \overline{\mathbf{F}_i} \\ \vdots \\ \overline{\mathbf{F}_{ns}} \end{bmatrix} \tag{23}$$

where the superior dot denotes a time derivative and each variable (e.g. P_c) is interpolated from the vector of nodal variables in the standard manner (i.e. $\overline{P_c} = \sum N_i \overline{P_{c_i}} = \mathbf{N}\overline{\mathbf{P}_c}$).

It is recognised that the continuous Galerkin method does not guarantee local mass conservation when applied to equations (21 & 22), and the system described by equation (23) may be subject to spurious oscillations;[39] particularly for an advection dominant case. To address this issue, a number of stabilisation techniques may be used, including mass lumping, SUPG and enrichment of the Galerkin method.[39-41] Alternatively, a different method could be employed for the spatial discretisation, such as the discontinuous Galerkin method.[39] In the present work, however, no spurious oscillations were observed in the problems considered and therefore it did not prove necessary to employ any of the above stabilisation techniques.

The global matrices are given by:

$$\overline{\mathbf{K}_{ij}} = \sum_{e=1}^{ne} \int_{\Omega^e} \nabla \mathbf{N}^{\mathrm{T}} \mathbf{K}_{ij} \nabla \mathbf{N} \, d\Omega^e \tag{24}$$

$$\overline{\mathbf{C}_{ij}} = \sum_{e=1}^{ne} \int_{\Omega^e} \mathbf{N}^{\mathrm{T}} C_{ij} \mathbf{N} \, d\Omega^e \tag{25}$$

$$\overline{\mathbf{F}_i} = \sum_{e=1}^{ne} \left(\int_{\Omega^e} \boldsymbol{\nabla} \mathbf{N} \cdot \mathbf{F}_{gi} \, d\Omega^e - \int_{\Omega^e} \boldsymbol{\nabla} \mathbf{N} \cdot \mathbf{F}_{di} \, d\Omega^e - \int_{\Gamma^e} \mathbf{N} F_{\mathrm{qi}} \, d\Gamma^e - \int_{\Omega^e} \mathbf{N} F_{\mathrm{Spi}} \, d\Omega^e \right) \tag{26}$$

where ne is the number of elements and the element matrices are as follows:

$$C_{11} = \frac{\partial (n S_w \rho_w)}{\partial P_c} + \frac{\partial (n S_g \rho_v)}{\partial P_c} \qquad C_{12}^i = 0$$

$$C_{21}^i = \frac{\partial (n S_w \rho_w c_i)}{\partial P_c} \qquad C_{22}^i = n S_w \rho_w$$

$$\mathbf{K}_{11} = -\rho_w \frac{\mathbf{K_{in}} K_{rw}}{\mu_w} + \mathbf{D}^{mv} \frac{\partial P_v}{\partial P_C} \qquad \mathbf{K}_{12}^i = \mathbf{0}$$

$$\mathbf{K}_{21}^i = -\rho_w \frac{\mathbf{K_{in}} K_{rw}}{\mu_w} c_i \qquad \mathbf{K}_{22}^i = \rho_w \mathbf{D}_i^d + n S_w \rho_w D_i^{mol} \mathbf{I}$$

$$\mathbf{F}_{g1} = \rho_w \frac{\mathbf{K_{in}} K_{rw}}{\mu_w} \rho_w \mathbf{g} \qquad \mathbf{F}_{\boldsymbol{g2}}^i = c_i \rho_w \frac{\mathbf{K_{in}} K_{rw}}{\mu_w} \rho_w \mathbf{g}$$

$$F_{q1} = q_v + q_w + \beta_c (\rho_v - \rho_v^{env}) \qquad F_{q2}^i = q_c + \gamma_c (c_i - c_i^{env})$$

$$F_{Sp1}^i = \left(\frac{\partial (n S_w \rho_w)}{\partial S_p^i} + \frac{\partial (n S_g \rho_v)}{\partial S_p^i} \right) \partial_t (S_p)_i \qquad F_{Sp2}^i = -n \rho_p \partial_t (S_p)_i$$

$$\mathbf{F_{d1}} = \mathbf{0} \qquad \mathbf{F}_{d2}^i = n S_w \rho_w D_i^{mol} \left(z_i c_i \frac{\sum_{i=1}^{ns} z_i D_i^{mol} \boldsymbol{\nabla} c_i}{\sum_{i=1}^{ns} z_i^2 D_i^{mol} c_i} \right)$$

The global system can be written in a compact form as:

$$\overline{\mathbf{K}} \boldsymbol{\Phi} + \overline{\mathbf{C}} \dot{\boldsymbol{\Phi}} = \overline{\mathbf{F}} \qquad \forall \, \mathbf{x} \in \Omega \tag{27}$$

Applying an implicit Euler backward difference scheme[33] for the time discretisation leads to:

$$\overline{\mathbf{K}} \boldsymbol{\Phi}^{t+1} + \frac{1}{\Delta t} \overline{\mathbf{C}} (\boldsymbol{\Phi}^{t+1} - \boldsymbol{\Phi}^t) = \overline{\mathbf{F}} \tag{28}$$

This set of nonlinear equations can then be solved using a standard Newton-Raphson procedure[33] based on a first order Taylor series expansion of the mass/energy balance error, which leads to the following incremental-iterative update of the primary variable vector ($\delta \boldsymbol{\Phi}_{k+1}^{t+1}$) :

$$\delta \boldsymbol{\Phi}_{k+1}^{t+1} = \left[\frac{\partial \boldsymbol{\varphi}}{\partial \boldsymbol{\Phi}_k^{t+1}} \right]^{-1} (-\boldsymbol{\varphi}) \tag{29}$$

where $\boldsymbol{\varphi}$ is the approximation error given here as:

$$\boldsymbol{\varphi} = \Delta t \overline{\mathbf{K}} \boldsymbol{\Phi}^{t+1} + \overline{\mathbf{C}} (\boldsymbol{\Phi}^{t+1} - \boldsymbol{\Phi}^t) - \Delta t \overline{\mathbf{F}} \tag{30}$$

Without a loss of generality, bilinear quadrilateral elements were used throughout this study.

Since convergence is not always guaranteed with the Newton-Raphson procedure,[39] the stability of a solution was checked using the following Courant-Friedrich-Lewy condition, as suggested by Zhu et al.[12]:

$$\frac{v_w \Delta t}{\Delta h} \leq 1 \tag{31}$$

4 Problem Reduction Scheme (PRS)

The balance equations governing reactive transport in porous media (eq. 27) are often highly coupled and nonlinear and, as such, the computational demand associated with their solution can become prohibitively expensive, particularly when solutions are required for large domains and relatively long time periods. The present approach addresses this issue by decoupling a number of the nonlinear PDEs from the global system of equations.

The proposed Problem Reduction Scheme (PRS) is a predictor-corrector approach that employs one or more indicator species and then, in the 'predictor' step, computes the transport of the other (non-indicator) species by interpolation. The 'corrector' step then refines the predicted concentrations using an error approximation. Reactions involving both indicator and non-indicator species are dealt with on a point-wise basis (at nodal points) at the end of each time step. Before describing the interpolations and detailed processes used in the PRS, the overall solution algorithm is presented to show where the PRS fits into the transient solution procedure.

4.1 Algorithm

Box 1 – Solution algorithm

Set $t = t_0$, $\boldsymbol{\Phi} = \boldsymbol{\Phi}_0$, $S_p = S_p^0$
Set boundary conditions (eqs. 19-20)
Undertake a linear solution for indicator species as a reference predicator i.e. Calculate c_i^{SIS} (eq. 35 or 36)
do itime=1,ntime ! Time step loop
  Increment time variable t
  do iiter=1,niter ! Iteration loop
    Calculate boundary fluxes (eqs. 17-18)
    Calculate reaction rates (eq. 15)
    Solve for incremental primary variables[1] $\delta\boldsymbol{\Phi}$ (eq. 29)
    Update primary variables $\boldsymbol{\Phi} = \boldsymbol{\Phi} + \delta\boldsymbol{\Phi}$
    if $|\boldsymbol{\Phi}|/\boldsymbol{\varphi}_{ref}$ <tol **then exit iteration loop**
  enddo iiter
  Apply 'Predictor' step (eq. 40). Compute the concentrations for non-indicator species.
  Apply 'Corrector' step (eq. 41). Compute the concentration correction for non-indicator species.
enddo itime

in which;
$\boldsymbol{\varphi}_{ref}$ = a reference vector for normalising the error ($\boldsymbol{\varphi}$)
ntime, niter are the number of time steps and limiting number of iterations respectively

Notes
[1] The primary variables comprise the capillary pressure and the concentrations of the indicator species

4.2 Formulation

The aim of the PRS scheme is to greatly reduce the computational cost of solving multi-species chemical transport problems by reducing the number of primary variables solved in the coupled system. In this scheme, a full solution is undertaken for the capillary pressure and a selected number of indicator species and then a predictor-corrector approach is used to compute the concentration of non-indicator species. The predictor first computes the concentration of non-indicator species from the concentration of the indicators and then a correction is applied to these values using an error approximation derived from an appropriate balance equation.

4.2.1 Predictor step

The concentrations of the indicator species at each time step are computed from the solution of the coupled equation system (eq. 27 and Box 1). Once these indicator concentrations are known, the predictor step is applied to compute the transport of non-indicator species. To derive this predictor step, the governing mass balance equation for a conservative chemical species i is considered, which, neglecting the charge neutrality condition, is given as:

$$\partial_t(nS_w\rho_w c_i) = -\boldsymbol{\nabla}\cdot(nS_w\rho_w c_i \mathbf{v}_w) + \boldsymbol{\nabla}\cdot\left(\rho_w \mathbf{D}_i^d\cdot\boldsymbol{\nabla}c_i + nS_w\rho_w D_i^{mol}\boldsymbol{\nabla}c_i\right) \quad (32)$$

where $\mathbf{D}_i^d$ is a function of the liquid moisture velocity and the dispersivities (see eq. 14).

Noting that both $\mathbf{D}_i^d$ and $\mathbf{v}_w$ are the same for all species, it can be seen from equation (32) that, for a conservative chemical species, the difference between the rate of transport of chemical species depends on their diffusion coefficients, concentrations and concentration gradients.

In the present study, Lagrangian polynomial interpolation is used for diffusion, with the interpolated diffusion being used to weight the change in concentration of an indicator species over a time step, Δc_{ind}, based on the relative difference between the known diffusion coefficients of the current non-indicator species D_i and of the indicator species D_{ind} and D_{jnd}, as follows:

$$g(D_i, \Delta c_{ind}) = \sum_{ind=1}^{n_{ind}} \Delta c_{ind} \prod_{jnd \neq ind, jnd=1}^{n_{ind}} \left(\frac{D_i - D_{jnd}}{D_{ind} - D_{jnd}} \right) \tag{33}$$

in which $g(D_i, \Delta c_{ind})$ is a diffusion interpolation function, which is incorporated into the final interpolation function below (eq. 34), n_{ind} equals the number of indicator species; subscripts ind and jnd denote specific indicator species, subscript i denotes non-indicator species; and D_i and D_{ind} represent the diffusion coefficient of any species and a specific indicator respectively. It can be noted that in the case of $n_{ind}=1$, eq. (34) simplifies to $g(D_i, \Delta c_{ind}) = \Delta c_{ind}(D_i/D_{ind})$.

Equation (33) does not account for the effect of the difference in concentration gradients between indicator and interpolated non-indicator species. This is addressed by introducing a concentration gradient function (f_c), and adding terms to account for chemical reactions and the charge neutrality condition, leads to equation (34) for predicting the concentration of a non-indicator species at time $t + \Delta t$:

$$c_i^{t+\Delta t} = c_i^t + \sum_{ind=1}^{n_{ind}} f_c \left(\frac{c_i^{gr}}{c_{ind}^{gr}} \right) \Delta c_{ind} \prod_{jnd \neq ind, jnd=1}^{n_{ind}} \left(\frac{D_i - D_{jnd}}{D_{ind} - D_{jnd}} \right) - \Delta t \partial_t (S_p)_i - f^{t+\Delta t} \tag{34}$$

where c_i is the concentration of a chemical species, c^{gr} refers to a concentration gradient, and the t superscript denotes time.

The penultimate term in equation (34) represents the source/sink (SS) due to chemical reactions and the final term (f) represents the diffusion due to the charge neutrality condition, which is elaborated in Section 4.3. In the scenario in which a reaction is 'sufficiently fast' in comparison with the rates of the transport processes, this may be treated under the local equilibrium assumption.[38] As such the change in concentration over a time step should be multiplied by a retardation factor, as detailed in Fetter,[42] (i.e. eq. (34) becomes $c_i^{t+\Delta t} = c_i^t + \frac{1}{R}\left(g(D_i, \Delta c_{ind}) - \Delta t \partial_t (S_p)_i - f^{t+\Delta t} \right)$ where R denotes the retardation factor for an equilibrium reaction and the SS term has been retained to account for any kinetic reactions).

A number of options were considered for the concentration gradient function (CGF) in eq. (34) (f_c), including using the ratio of non-indicator to indicator gradients from the previous time step and using a weighted measure of concentrations from the sources. Both of these options proved to be flawed and to have problem-dependent levels of accuracy. A more successful approach was to derive f_c from a 'source influence solution' (SIS), which is a linear steady state solution of the diffusion problem for each chemical species that is carried out at the beginning of the solution procedure (thereby having a negligible effect on the overall solution time) and is given as:

$$\boldsymbol{\nabla} \cdot \left(-n S_w \rho_w D_i^{mol} \boldsymbol{\nabla} c_i^{SIS} \right) = 0 \tag{35}$$

noting that n, ρ_w and D_i^{mol} are constants, for a uniformly saturated medium eq. (35) simplifies to the Poisson equation:

$$\nabla^2 c_i^{SIS} = 0 \tag{36}$$

The output from the SISs are the concentrations of each chemical species throughout the domain, which are subsequently employed in f_c as follows:

$$f_c\left(\frac{c_i^{gr}}{c_{ind}^{gr}}\right) = \frac{c_i^{SIS} - c_i^0}{c_{ind}^{SIS} - c_{ind}^0} \tag{37}$$

4.2.2 Corrector step

The corrector refines the concentrations computed from the predictor step using the mass balance approximation error (eq. 30) for each non-indicator species in turn. The concentration correction for each species i is then based on a first order Taylor series expansion of a single species form of equation 29, as follows:

$$\mathbf{c}_{err_i} = \left(\overline{\mathbf{M}_i}\right)^{-1} \boldsymbol{\varphi}_i \tag{38}$$

where $\mathbf{c}_{err_i}$ is the concentration correction vector for species i and $\overline{\mathbf{M}_i}$ is an approximate tangent coefficient matrix.

Two forms of $\overline{\mathbf{M}_i}$ were considered as follows:

Option 1: $\overline{\mathbf{M}_i} = \overline{\mathbf{C}_{diag_i}} + \Delta t \overline{\mathbf{K}_{diag_i}}$

Option 2: $\overline{\mathbf{M}_i} = \overline{\mathbf{C}_{diag_i}}$

in which $\overline{\mathbf{C}_{diag_i}}$ is the lumped diagonal storage matrix and $\overline{\mathbf{K}_{diag_i}}$ is a diagonal form of the flux matrix.

The use of diagonal lumped matrices implies that the concentrations can be updated on a point-wise basis. The concentrations are refined as:

$$c_{cor_i}^{t+\Delta t} = c_{pre_i}^{t+\Delta t} - c_{err_i} \tag{39}$$

It was found that the two options gave similar results in terms of the accuracy of solutions and therefore the simpler option (2) was adopted for all subsequent computations. In this study, the corrector step was treated as non-iterative since it was found that sufficient accuracy could be obtained using a single corrector step, as illustrated in Sections 6 and 7 of this paper.

4.2.3 Summary of predictor-corrector scheme

In the present work, three different orders of the generalised reduction scheme are investigated, denoted PRS0, PRS1 and PRS2, which use 1, 2 and 3 indicator species respectively. Recalling equations (34 & 39), the predictor-corrector scheme is summarised as:

$$c_i^{t+\Delta t} = c_i^t + \sum_{ind=1}^{n_{ind}} f_c\left(\frac{c_i^{gr}}{c_{ind}^{gr}}\right) \Delta c_{ind} \prod_{jnd \neq ind, jnd=1}^{n_{ind}} \left(\frac{D_i - D_{jnd}}{D_{ind} - D_{jnd}}\right) - \Delta t \partial_t \left(S_p\right)_i - f^{t+\Delta t} \tag{40}$$

$$c_{cor_i}^{t+\Delta t} = c_{pre_i}^{t+\Delta t} - c_{err_i} \tag{41}$$

4.3 Boundary conditions and charge neutrality condition

The initial conditions for the PRS can be defined in the same way as in the full model (i.e. using equation (16) for all species). The boundary conditions for the PRSs are also defined in the same way as for the full model and should be of the same type for both 'indicator' and 'non-indicator' species, with the latter being calculated on a point-wise basis.

Another key consideration is how the charge neutrality condition is satisfied in the PRSs, since the transport of non-indicator species is not calculated in the reduced system of governing equations. In the present approach, the diffusive flux due to the electric field is considered explicitly by using concentrations from the previous time step and moving these to the right hand side of the governing equations in a similar manner to the way that moisture flow under gravity is included in liquid transport computations. For non-indicator species, this can then be calculated on a point-wise basis and subtracted at the end of a PRS predictor step (eq. 40). The diffusive flux due to the electric field is therefore given by:

$$f^{t+\Delta t} = \nabla \cdot \left(-S_w D_i^{mol} z_i c_i \frac{\sum_{i=1}^{ns} z_i D_i^{mol} \nabla c_i}{\sum_{i=1}^{ns} z_i^2 D_i^{mol} c_i} \right)^t \tag{42}$$

4.4 Selection of indicator species

The choice of indicator species is an important aspect of the PRS. For PRS1 and PRS2, species with the highest and lowest diffusion coefficients are always defined as indicators. This ensures that the computed responses of all non-indicator species are bounded by those of fully computed species. For PRS2, which requires a third indicator species, it was found, following an error analysis and sensitivity study (see section 6.2), that the greatest accuracy was achieved by using a third indicator species with a mean diffusion coefficient . In cases where such a real species is not available, artificial species can be used. Artificial indicator species may also be used for other reasons; for example, as mentioned above, PRS1 and PRS2 use indicator species with the highest and lowest diffusion coefficients. However, the presence of any reactions associated with one of the bounding species, with reaction rates of the same order as (or higher than) those of the transport processes, may alter its rate of transport, such that it may no longer be the highest/lowest. In such situations, a non-reactive artificial indicator should be used in its place, thereby maintaining the solution bound. The criterion used to select the single indicator species required for PRS0 is given in Section 6.2

Another aspect of reactive transport problems, which is relevant to the choice of the indicator species, is that the transport of different species can take place over very different time scales. When this occurs due to a dominant (or 'sufficiently fast'[38]) reaction linked to a particular non-indicator species, this is dealt with by modelling the process as an equilibrium reaction. If this is due to other factors, then indicator species could be chosen to represent each different time scale.

It is recognised that other factors may also affect the choice of indicators; however, the factors considered in the present work encompass a wide range of real problems.

The number of indicator species, and associated order of the scheme, is also a key consideration when employing the PRS. The choice of the number of indicator species to use depends upon the problem under consideration, and specifically upon the range of diffusion coefficients of the chemical species in the system. In general, the smaller this range, the lower the order of the scheme that is required, with PRS0 being applicable to problems in which the diffusion coefficients lie in a narrow range, as

quantified in Section 6.2. An exception to this rule is problems with a significant degree of advection, for which PRS0 is not appropriate (unless the diffusion coefficients are equal for all species), since solutions for the non-indicator species transport are not bounded, which can lead to an overestimation of the advection.

The specific selection criteria used to determine the indicators for each order of PRS is given in Section 6.2, along with the expected accuracy for each degree of scheme.

5 Validation of the full model

Before investigating the behaviour of the PRS, the validity of the full model is demonstrated. To this end, a non-steady-state diffusion problem reported by Baroghel-Bouny et al.[35] is considered. This problem is based on experiments carried out by Francy[43] on cement discs of 120(d)x20(h) mm. In these tests, the left hand side of the sample was exposed to a salt solution whilst the remaining sides were sealed. The transport of Na^+, OH^-, K^+ and Cl^- ions was considered and non-equilibrium chloride binding was also taken into account, using eq. (15), in addition to the instantaneous formation of Friedel's salt. It is assumed that since chloride ions sorb onto the solid mass, hydroxide ions are released to preserve charge neutrality. At the end of the test, measurements were taken of the free chloride and total chloride content of the sample at different locations.[35,43] The problem set up can be seen in Figure 1.

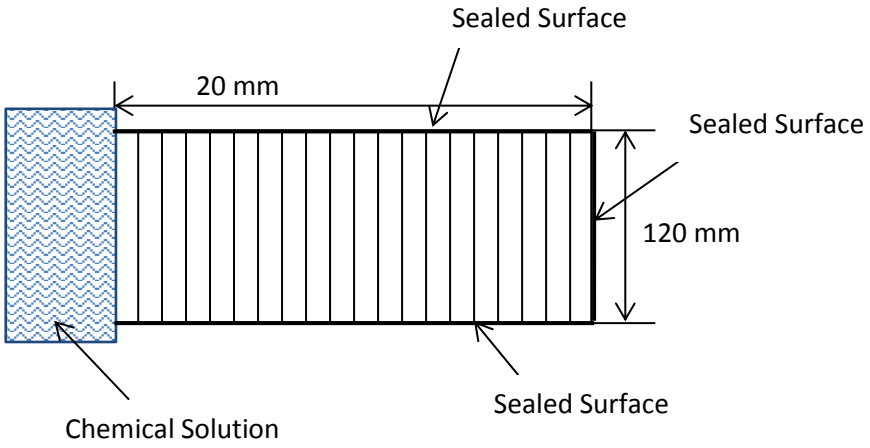

Figure 1 – Finite element mesh and problem geometry (not to scale)

The time period considered was 7 days and, following a mesh and time step convergence study, a time step of $\Delta t = 3.6\ s$ was selected, giving a total number of time steps of 168,000, along with a mesh of 20 bilinear quadrilateral elements with a maximum element size of 1 mm. To reflect experimental conditions, the sample was assumed to be initially saturated. The model parameters, boundary conditions and diffusion coefficients of the chemical species are given in Table 1. It should be noted that in this example it was found that a tortuosity factor, $D_{\tau,}$ was needed to correctly predict the chemical transport; this factor takes into account the tortuous pathways of the medium and is simply multiplied by the species diffusion coefficients.

Table 1 – Model parameters

Parameter	Value	Species	Initial Conc. (kg/kg)	Boundary Conc. (kg/kg)	D^{mol} $(10^{-11} m^2/s)$
n	0.13	Na^+	0.000299	0.01352	1.33
$\gamma_c\ (kg/m^2 s)$	6.5×10^{-3}	OH^-	0.001105	0.00188	5.3
D^τ	0.5	K^+	0.002028	0.00319	1.96
μ	2.61	Cl^-	0.0	0.01954	2.1
λ	0.61				
$\tau\ (s)$	36000				
$p_C^0\ (kN/m^2)$	1.34×10^3				

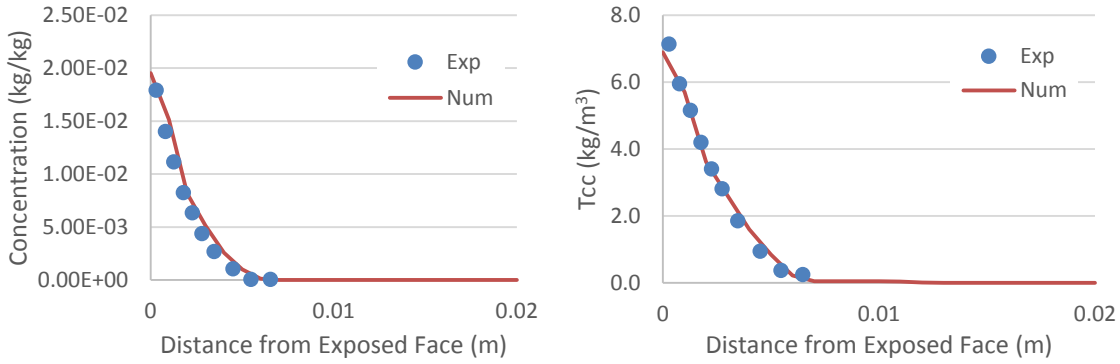

Figure 2 – Cl^- concentrations and Tcc profiles as predicted by the full model at t=7 days (where Tcc is measured in kg/m^3 of mortar)

The concentration profile and total chloride content (Tcc), as predicted by the full model, are compared with the corresponding experimental results in Figure 2. The numerical results are considered sufficiently close to the experimental results to validate the full model. The CPU time for the simulation was 1382 s.

6 Investigation of the range of applicability

The accuracy and range of applicability of the PRS with three different orders of the scheme (namely PRS0, PRS1 and PRS2) is studied by considering a wick action test on a mortar sample in which the transport of 16 chemical species is simulated. The analysis undertaken in this study considered chemical reactions between the ions and the cement matrix, as well as advective and dispersive transport. It was decided to use an artificial set of chemical species for this study in order to have control over the range and spread of the diffusion coefficients considered.

The reactions concerned the adsorption of the chemical ions onto the cement matrix, described by the non-equilibrium Freundlich isotherm (eq. 15). The time period considered was 24 hours and the initial concentration of each ion, as well as the sorbed chemical mass for each species in the sample, was assumed to be zero. The mortar sample was assumed to be initially saturated, prior to the left hand side of the specimen being exposed to the chemical solution, and the right hand side being exposed to an environmental humidity of 60 %, with all remaining sides being sealed, thereby ensuring 1D transport. A non-uniform mesh of 25 bilinear quadrilateral elements was used along the length of the specimen, with a maximum element size of 4 mm. A time step of $\Delta t = 36\ s$ was used, giving a total

number of time steps of 2,400. As with the previous validation case, the mesh and time step were adopted following a convergence study.

The diffusion coefficients for all species can be seen in Table 2, whilst model parameters, including the boundary mass transfer coefficients for all chemical species, are given in Table 3.

Table 2 – Diffusion coefficients

Species	D^{mol} (10^{-10} m^2/s)	Species (cont'd)	D^{mol} (10^{-10} m^2/s)
1	0.25	9	6
2	0.5	10	7
3	1	11	8
4	1.5	12	9
5	2	13	10
6	3	14	12
7	4	15	14
8	5	16	16

Table 3 – Model parameters

Parameter	Value	Parameter	Value
μ	16	K_{in} (m^2)	35×10^{-21}
λ	2.0	c^{b*} (kg/kg)	1×10^{-3}
τ (s)	2000	z^* (-)	1
n	0.13	c^{0*} (kg/kg)	0.0
β_c (m/s)	2.5×10^{-3}	p_c^0 (kN/m^2)	1.34×10^{3}
γ_c (kg/m^2s)	1×10^{-4}		

*for all species

6.1 Full-model results

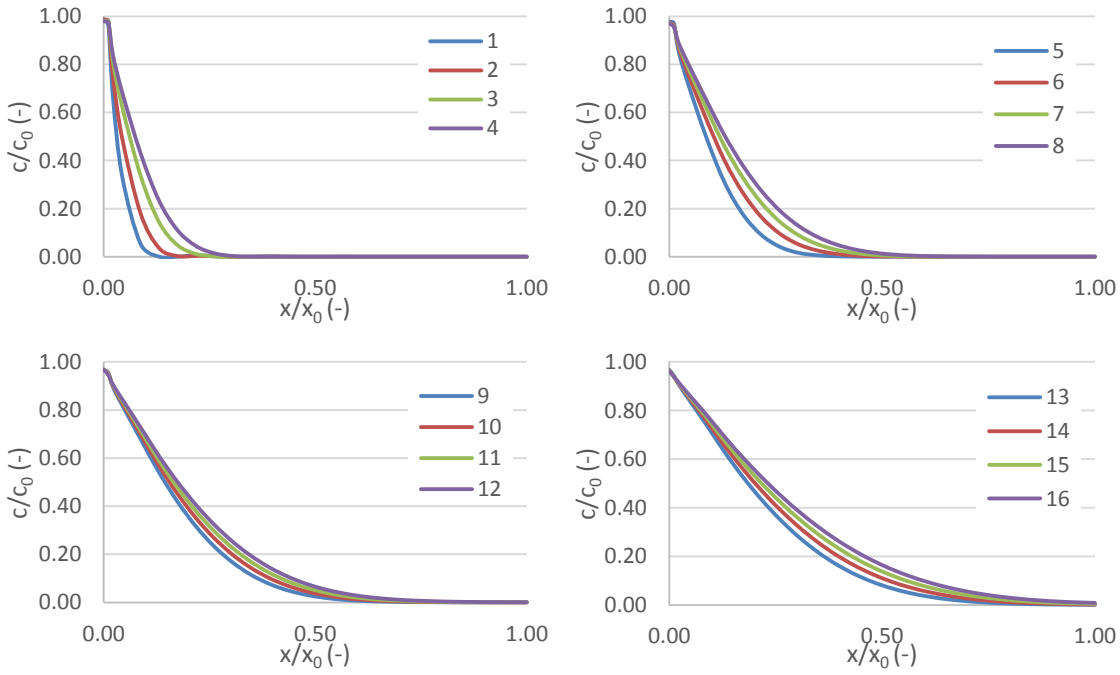

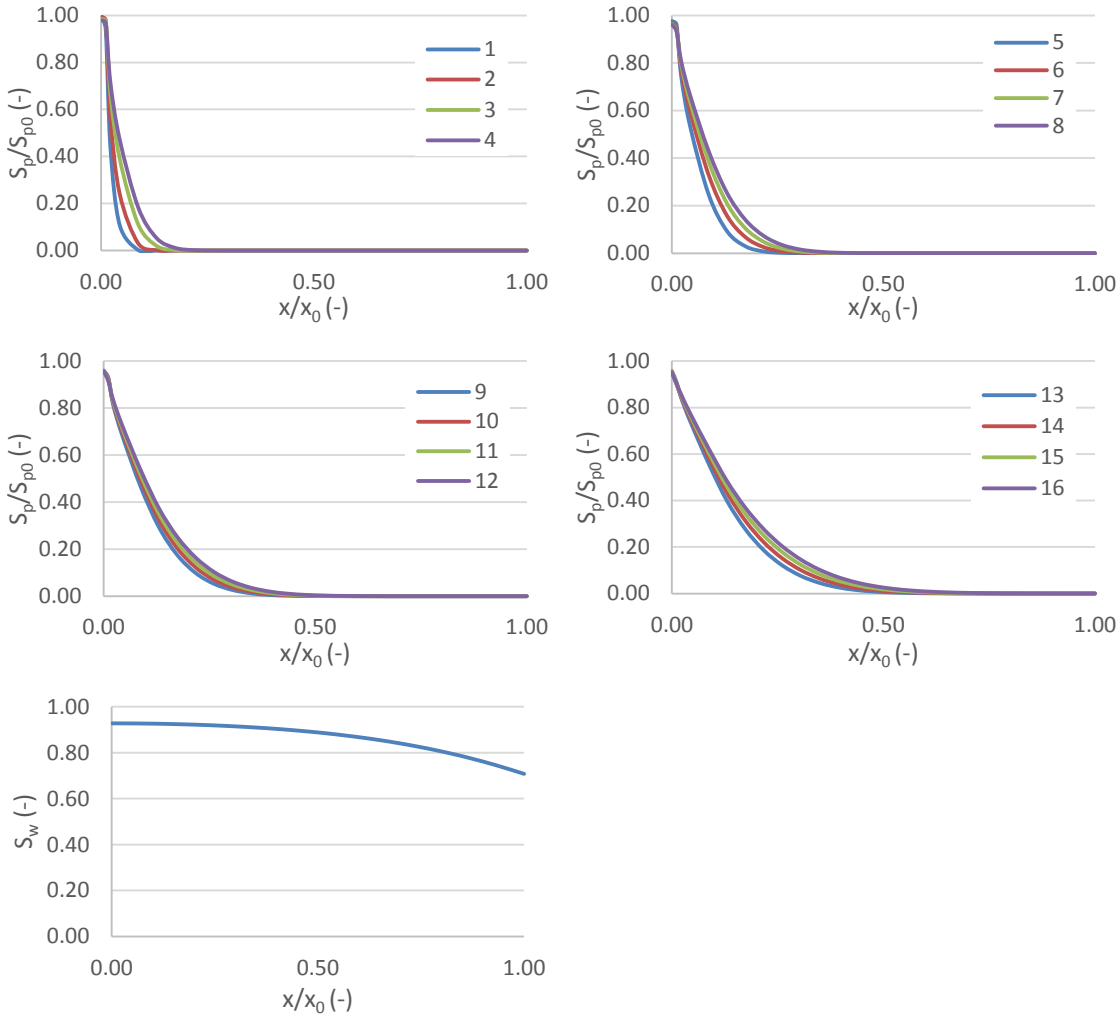

Figure 3 – Normalised concentration, sorbed mass profiles and saturation profile as predicted by the full model at t=24 hrs

To determine the accuracy of the reduction schemes, an analysis of the full problem was undertaken. The calculated profiles of chemical concentration, moisture content and sorbed masses from this full analysis at time $t=24\,hrs$ are given in Figure 3. The responses are plotted in groups of species in order of increasing diffusion coefficient (D^{mol}). The relative difference between the four responses in each of the groups reflects the relative spread of diffusion coefficient across the group, with group 1 (species 1 to 4) representing a six fold increase in diffusion coefficient and group 4 having a relative increase of only 1.6. The moisture profile shows that some drying of the specimen has occurred over the 24 hour analysis period but most of the sample remains saturated or near-saturated. The sorbed mass profiles are very similar to the concentration profiles but with less penetration into the sample. The CPU time for the simulation was 312s.

6.2 PRS results

In this section, the results from a set of analyses of the problem considered in Section 6.1, undertaken with the three orders of PRS, are compared with the results from the full analysis described above. The indicator species chosen for each of the solutions are presented in Table 4. An artificial species labelled 'A' has been chosen for PRS0 and PRS2 in order to allow the use of an indicator with a diffusion coefficient corresponding to the mean value of the species diffusion coefficients.

Table 4 – Indicator species chosen and the corresponding diffusion coefficients (10^{-10} m^2/s)

PRS	Indicator 1	Indicator 2	Indicator 3
0	A (6.2)	-	-
1	3 (1)	9 (6)	-
2	3 (1)	A (7.03)	16 (16)

This problem is used to determine the range of applicability of each of the reduction schemes based on a maximum allowable error in any one chemical species at any one time. The tolerance measure considered is the mean absolute percentage error (MAPE), defined as:

$$MAPE = \frac{100}{n} \cdot \sum_{i=1}^{n} \left| \frac{c_i^{prs} - c_i^{full}}{c_i^b} \right| \tag{43}$$

An acceptable MAPE of 3 % was selected for PRS0, and 1 % for both PRS1 and 2 to enable the definition of the range of applicability of each scheme. It is acknowledged that these tolerances are a matter of judgement and that different problems will require different levels of accuracy. 1 % is considered to be a reasonable tolerance for most practical purposes and 3 % is thought to be an acceptable error for the type of relatively coarse approximation associated with PRS0.

For PRS0, it is possible to consider species with progressively larger or smaller diffusion coefficients until a profile exceeds the tolerance; however, this is not possible for PRS1 and PRS2 as they use the extremes of the diffusion coefficient range as indicator species. To overcome this issue, the range was successively varied on a trial and error basis until the maximum range that meets the tolerance was found.

The resulting ranges, over which each PRS achieves the selected tolerance, are given in Table 5 (where the u and l superscripts indicate upper and lower indicators respectively). The intermediate indicator ($D_{ind,m}$) for PRS2 was chosen to be the mean diffusion coefficient, which was based on the results of a series of analyses aimed at finding the value of $D_{ind,m}$ that produced the most accurate solutions.

Table 5 – Diffusion coefficient ranges over which each scheme is applicable

PRS	0	1	2
Diffusion Coefficient Range	$0.8D_{ind}<D_i<1.5D_{ind}$	$D_{ind,u}<6D_{ind,l}$	$D_{ind,u}<16D_{ind,l}$*

*the maximum MAPE was 1.13 %, but this was deemed close enough to the 1 % tolerance, the average was only 0.63 %

To further explore the influence of changing the diffusion coefficient of an indicator species, a sensitivity analysis was undertaken on the value of the diffusion constant used for the intermediate indicator for PRS2. Using the problem considered in Section 6.1, it was found that changing this coefficient by 20 % resulted in an increase in the MAPE of 0.13 % and the mass balance error of 0.17 %, which suggests that the scheme is relatively insensitive to the choice of the intermediate indicator.

Profiles showing the two species with the largest departure from results of the full analysis, within the range of applicability given in Table 5, are presented for each PRS scheme in Figure 4. The relative percentage error plots for each PRS can be seen in Figure 5, where the relative percentage error is given as: $RE = \left|\left(c_i^{prs} - c_i^{full}\right)/c_i^b\right|$. It can be seen from the profiles that PRS results are very close to

those of the full model, particularly for PRS1 and 2. The profiles corresponding to the PRS without the corrector step show a larger departure from the results of the full analysis; however, the profiles are still relatively close to one another. This shows that for this particular problem, the corrector has a limited effect, although, as is shown in Section 7.1, this is not the case for many other problems.

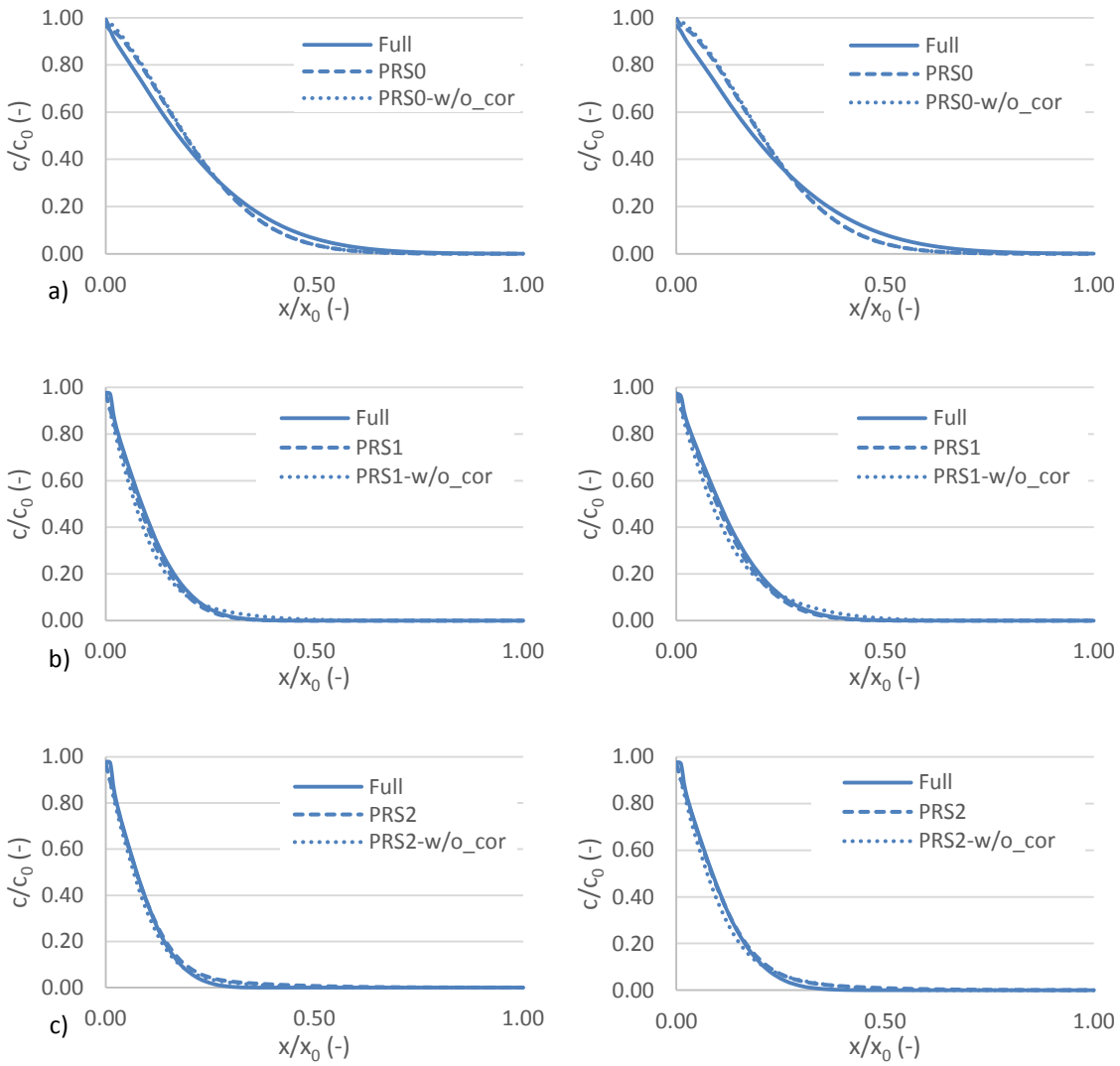

Figure 4 – Worst case profiles in applicable range for a) PRS0 (species 12 & 13), b) PRS1 (species 5 & 6) and c) PRS2 (species 4 & 5) at t=24 hrs

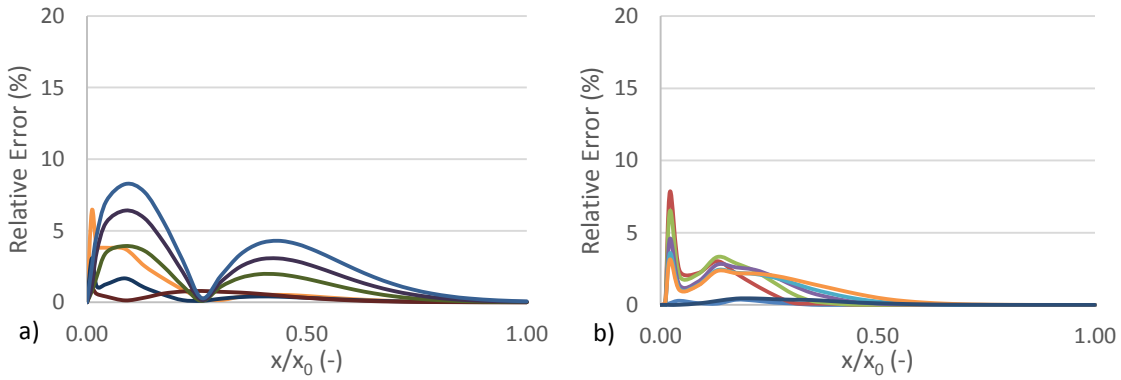

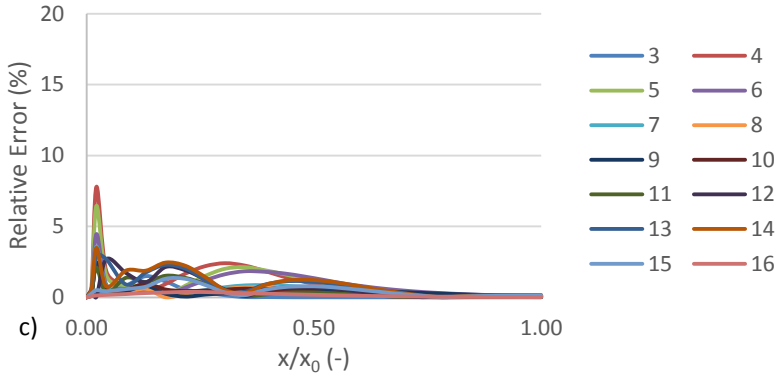

Figure 5 – Relative error profiles for a) PRS0, b) PRS1 and c) PRS2

As well as the relative error in concentrations, another key consideration is the mass balance error. To assess this, the total accumulated mass balance error was calculated by comparing the mass of each chemical in the system obtained from the PRS analysis with the results from the corresponding full analysis; the latter being taken as the correct solution for this purpose. The average relative mass balance errors were 1.14 % for PRS0, 4.24 % for PRS1 and 1.98 % for PRS2. In this case, the mass balance error for PRS0 is the smallest, even though PRS0 predicts the concentrations less accurately. This is because PRS0 has areas of over-prediction and under-prediction, leading to a small overall error in mass balance.

The results of this investigation led to the PRS selection criteria for the PRS given in Tables 6 and 7. These recommendations are based on the range of diffusion coefficients for each scheme, which was found to give an acceptable MAPE, and the corresponding indicator species selected. The selection of the order of the PRS scheme should also take into account the fact that PRS0 is an inappropriate choice for problems with a significant degree of advection, as discussed in Section 4.4. Clearly it would be possible to use higher order PRSs, but the range of orders examined here (i.e. 0 to 2) are considered to cover the majority of practical examples.

Table 6 – Selection of order of PRS

Diffusion Coefficient Range	PRS scheme
$\boldsymbol{D_u}$<1.9$\boldsymbol{D_l}$	0**
$\boldsymbol{D_u}$<6.0$\boldsymbol{D_l}$	1
$\boldsymbol{D_u}$<16$\boldsymbol{D_l}$	2

*where D_u and D_l indicate the upper and lower diffusion coefficients respectively
**where advection is significant, PRS1 is the appropriate choice

Table 7 – Selection of indicator species for each order of PRS

PRS scheme	Indicator number		
	1	**2**	**3**
0	$0.67D_u$**	-	-
1	D_l	D_u	-
2	D_l	D_{mean}	D_u

*where the selected indicator species should have diffusion coefficients corresponding to the tabulated values, in the case that no species exists with such a diffusion coefficient, or the species is highly reactive, an artificial species with corresponding diffusion coefficient should be used
**this recommendation is based on the fact that PRS0 was found to have an upper limit to its applicable diffusion coefficient range of $1.5D_{ind}$ (see Table 5)

6.2.1 Convergence

The above problem (described in Section 6.1) was also used to examine the convergence properties of the model with respect to mesh refinement (i.e. h refinement) and with respect to the order of the PRS (or PRS-order). The following L^2 error norm was employed in these convergence studies:

$$\|\mathbf{e}\|_{L^2} = \|\mathbf{c} - \mathbf{c}^r\|_{L^2} \tag{44}$$

where $\mathbf{e}$ is the error vector and $\mathbf{c}^r$ is the vector of reference concentrations.

In the absence of an analytical solution to this problem, the reference solution for the h-convergence study was obtained by using a very fine mesh (h=3.125x10^{-4} mm); for example, the reference solution for PRS0 is the PRS0 solution obtained using this very fine mesh.

The reference solution for PRS-order convergence was the solution from the full model. The results of the investigation are given in Figure 6. It is noted that uniform meshes were used for all of the analyses in this convergence study and that the mesh size for the PRS-order convergence was h=6.25x10^{-4} mm.

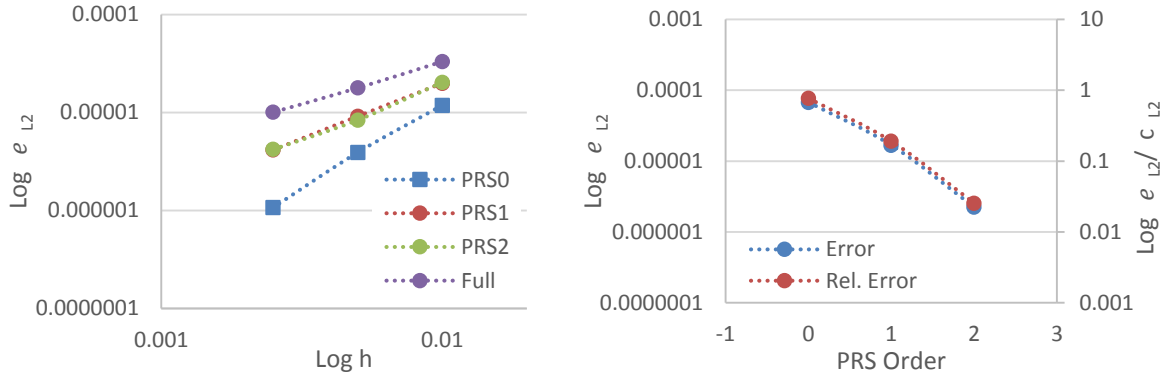

Figure 6 – Mesh size and PRS order convergence study results

The results presented in Figure 6 show that the full model and all PRSs exhibit satisfactory h-convergence. It noticeable that that the order of h-convergence is greatest for PRS0 but least for the full solution, but this believed to relate to the fact that the reference solutions for each set of results are those obtained from a fine mesh with the order of scheme being considered. The 'error' measures are therefore relative and not absolute.

The results also show the convergence with respect to PRS-order. It is interesting to note that the relative errors of the PRS solutions are similar to those of the reduced order model (ROM) of the reactive advection-diffusion equation found in McLaughlin et al.[44] and of the solute transport problem found in Luo et al.[45] In addition to this, the convergence with respect to PRS-order shows similarities to the convergence of aforementioned ROMs with respect to the number of basis functions employed.

7 Validation of the PRS

Having established a range of applicability for each PRS-order, it is considered desirable to validate the final procedure using data reported by other authors. To this end, a problem for each reduction order has been considered in addition to an advection dominant problem for PRS1 and PRS2. The first two problems consider the diffusion and reactions of chemical species in a mortar sample and are based on alternative numerical solutions presented by previous authors.[35,36] The third example is a

hypothetical scenario and considers 2D diffusive-reactive transport in a mortar specimen based on the example in Zhu et al.[12] The advection dominant problem is an extension of the advective example reported in Baroghel-Bouny et al.[35]

As before, the meshes and time steps used for all of the analyses reported in this section resulted from convergence studies.

7.1 PRS0

The diffusion case reported by Baroghel-Bouny et al.[35], which was used to validate the full model, is considered here over a time period of 12 hours, using the same mesh and time step as reported in Section 5. The total number of time steps was 12,000. The sample was assumed to be initially saturated.

The narrow range of the diffusion coefficients of the dominant species in this problem suggests that PRS0 is applicable. The chosen indicator species was Na^+ and the diffusion coefficients for non-indicator species K^+ and Cl^- lie within the established range of validity of PRS0; however, the other species, OH^-, lies outside the nominal applicability range but since there is little transport of OH^-, this was deemed acceptable in this case. The model parameters, boundary conditions and diffusion coefficients of the chemical species can be seen in Table 1, with the one difference being that a value of $\tau = 360\ s$ was used for the chloride binding.

The concentration profiles as predicted by the full model and PRS0 can be seen in Figure 7, along with the total chloride content (Tcc).

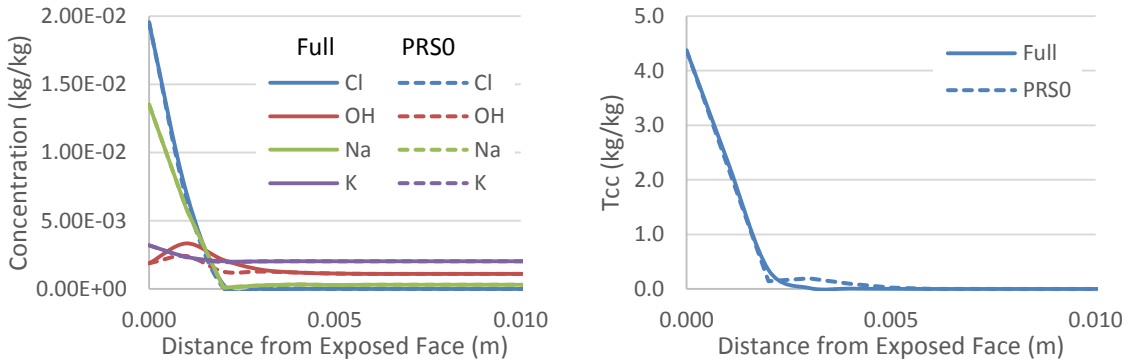

Figure 7 – Chemical concentrations and Tcc profiles as predicted by the full model and PRS0 at t=12 hrs

It can be seen from the profiles that the PRS results show a very close match to those of the full model, with the exception of the OH^- profile, which involves a relatively small overall change in concentration. The reason for the greater difference observed in the predicted OH^- profiles is that the diffusion coefficient lies outside of the applicable range of the scheme; as such, the transport is being over-predicted by PRS0 and the local peak of OH^- ions dissipates more quickly than in the full model simulations. The average relative mass balance error in this analysis is 2.05 %.

The Cl^- concentration profiles predicted by the full model and PRS0 with and without the corrector step are shown in Figure 8. It may be seen from the profiles that in this example the corrector step has a significant effect on the accuracy of the solution, with the profile predicted by PRS0 without the corrector showing a much greater departure from that predicted by the full model. In addition to this,

neglecting the corrector step increases the average relative mass balance error in this analysis to 8.31 %. The CPU times using the full model and PRS0 were 101 s and 62 s respectively.

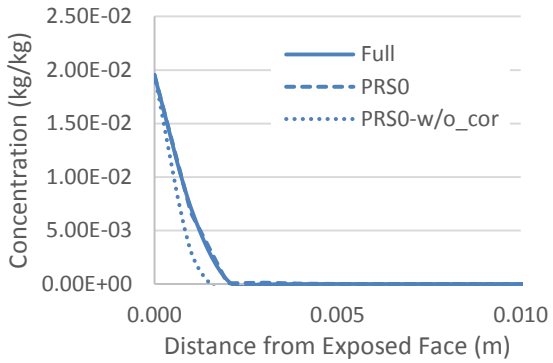

Figure 8 – Cl^- concentration profiles as predicted by the full model, PRS0 and PRS0 without corrector at t=12 hrs

7.2 PRS1

Diffusion experiments, and accompanying numerical simulations, presented by Song et al.[36] are considered here. In these tests, a concrete slab was cured for 90 days, after which a series of 100(d)x50(h) mm cylindrical cores were taken from the slab. The sides and bottom of the specimens were then sealed and the remaining surface exposed to a salt solution for 6 months. The simulation considers the transport of six chemical species (OH^-, K^+, Na^+, Cl^-, SO_4^{2-}, and Ca^{2+}). The reaction rates for the chemical species were considered as given by:

$$r_1 = k_d^{CSH.CaCl_2}[CSH.CaCl_2] - k_a^{CSH.CaCl_2}([Ca^{2+}][Cl^-]^2)^{\lambda_1} \quad (45)$$

$$r_2 = k_d^{CSH.NaCl}[CSH.NaCl] - k_a^{CSH.NaCl}([Na^+]^2[Cl^-]^2)^{\lambda_2} \quad (46)$$

$$r_3 = k_d^{CSH.2KCl}[CSH.2KCl] - k_a^{CSH.2KCl}([K^+]^2[Cl^-]^2)^{\lambda_3} \quad (47)$$

$$r_4 = k_d^{CSH.2NaOH}[CSH.2NaOH] - k_a^{CSH.2NaOH}([Na^+]^2[OH^-]^2)^{\lambda_4} \quad (48)$$

$$r_5 = k_d^{CSH.2KOH}[CSH.2KOH] - k_a^{CSH.2KOH}([K^+]^2[OH^-]^2)^{\lambda_5} \quad (49)$$

$$r_6 = k_d^{CAH.CaCl_2}[CAH.CaCl_2] - k_a^{CAH.CaCl_2}([Ca^{2+}][Cl^-]^2)^{\lambda_6} \quad (50)$$

where k_a and k_d represent the adsorption and desorption rates respectively. The Freundlich type isotherm was used and the adsorption calculated based on a non-equilibrium assumption. The SS term for the mass balance equation (eq. 8) for each species is given as the sum of the SS due to each relevant reaction (e.g. the SS for Ca^{2+} is obtained from: $\partial_t(S_p)_{Ca} = r_1 + r_6$). Song et al.[36] also considered the reaction of the cement matrix minerals; however, the associated changes were negligible and these reactions were therefore not included in the present computations.

The model parameters are given in Table 8. The boundary conditions are given in Table 9 along with the diffusion coefficients and the D^{es} factors which account for electrostatic double-layer effects[36]. The sample was assumed to be initially saturated and the time period considered was 2 months. The time step size was $\Delta t = 36\ s$, giving a total number of time steps of 144,000, and a mesh of 52 bilinear quadrilateral elements was used with an element size of 2 mm. PRS1 was applicable since the diffusion

coefficient range satisfies the condition ($D_{ind,u}$<6$D_{ind,l}$), the OH^- and K^+ species were chosen as the indicator species in this case as they are the species with the highest and lowest effective diffusion coefficients respectively (where the effective diffusion coefficient is given as the product of D^{mol} and D^{es}).

Table 8 – Model parameters

Parameter	Value
n	0.13
$\gamma_c\ (kg/m^2s)$	$1x10^{-4}$
$p_c^0\ (kN/m^2)$	$1.34x10^3$

Table 9 – BCs, ICs and diffusion coefficients of chemical species

Species	Initial Conc. (kg/kg)	Bound. Conc. (kg/kg)	D^{mol} $(10^{-9}m^2/s)$	D^{es}	Eq.	$k_a\ (10^{-8})$	$k_d\ (10^{-8})$	λ
Na^+	0.001978	0.0	1.33	0.25	*r1*	18.0	12.0	0.35
OH^-	0.004573	0.0	5.3	0.25	*r2*	24.0	144.0	0.35
K^+	0.007215	0.0	1.96	0.0875	*r3*	330.0	1375.0	0.35
Cl^-	0.0	0.01775	2.1	0.25	*r4*	1.275	6.42	0.2
SO_4^{2-}	0.000192	0.0	1.07	1.0	*r5*	0.75	5.4	0.2
Ca^{2+}	0.00004	0.01	0.79	0.4	*r6*	1000.00	1200.0	0.35

The concentration and sorbed mass profiles as predicted by the full model and PRS1 can be seen in Figure 9. The results of the PRS solution are a close match to those of the full model. The largest difference can be seen in the Cl^- profile, which is due to the fact that Cl^- ions are very reactive in this case being involved in 4 of the 6 reactions. The average relative mass balance error in this analysis is 2.23 %. The CPU times using the full model and PRS1 were 409 s and 198 s respectively.

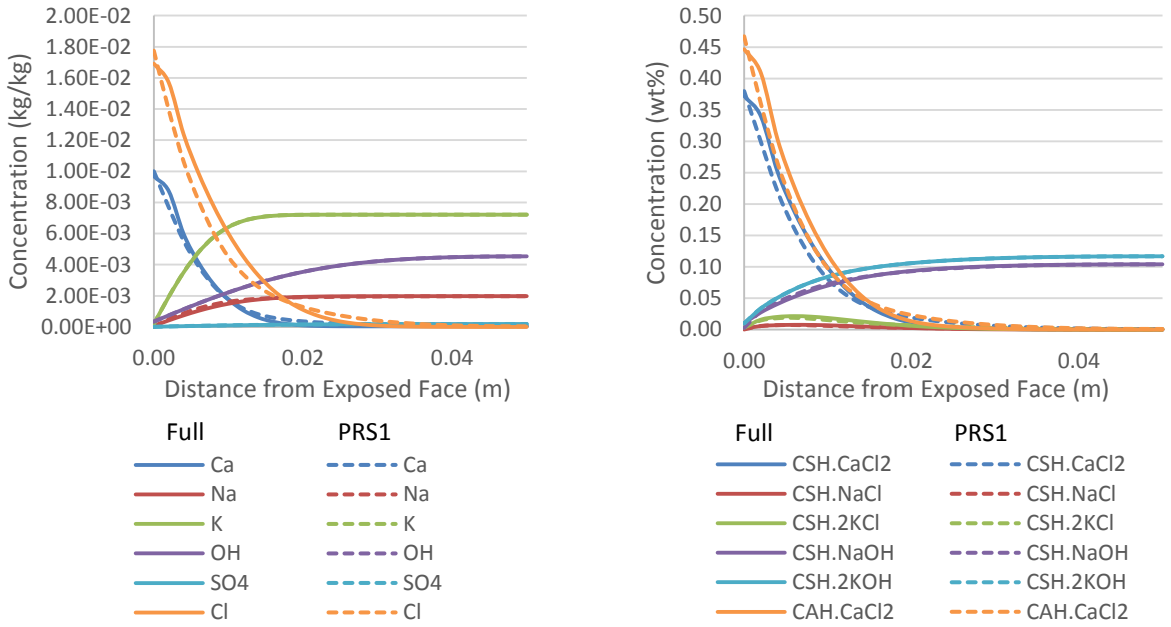

Figure 9 – Chemical concentrations and sorbed mass profiles as predicted by the full model and PRS1 at t=2 months (where sorbed mass concentrations are measured in wt% of concrete, sorbed masses containing Cl are measured in Cl concentration of the sorbed mass in wt% of concrete)

7.3 PRS2

The third simulation is based on a study by Zhu et al.[12]. This involves the transport of 10 chemical species, precipitation of 6 minerals and considers 1 immobile solid species. This is a 2D problem with a point and a line source for the chemical species (marked A and B respectively in Figure 10; point A corresponds to the coordinates (0,0), whilst the two ends of line B correspond to the coordinates (15,4) and (15,8) respectively). The geometry of the problem is given in Figure 10. The boundary conditions impose a zero flux on all sides. The time period considered was 24 hours, $\Delta t=36\ s$, giving a total number of time steps of 2,400, and a mesh of 1000 bilinear quadrilateral elements was used with an element size of 0.5 mm (as shown in Figure 10). It was assumed that the sample was initially saturated.

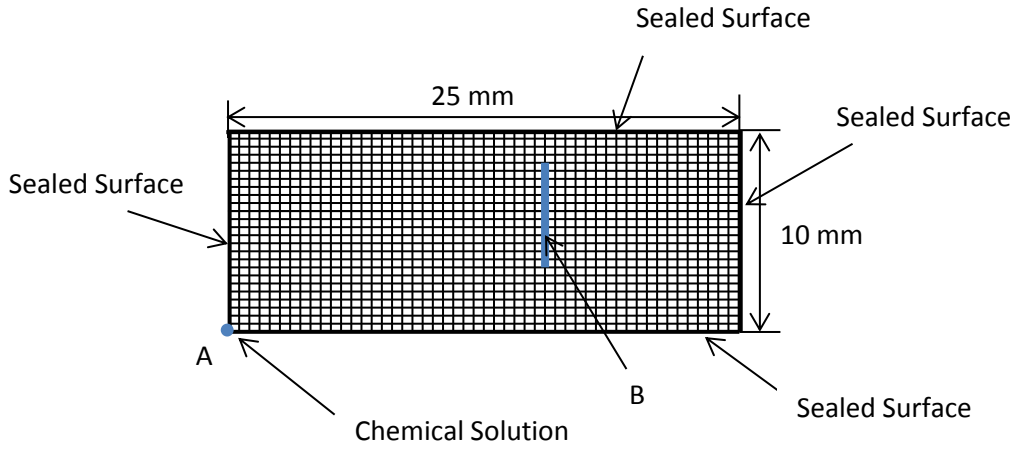

Figure 10 – Problem geometry (not to scale)

The Freundlich type isotherm (eq. 15) was used and the reactions were calculated based on a non-equilibrium assumption. The reaction rates for the 6 solid minerals considered are given as:

$$r_1 = k_d^{Al(OH)_3}[Al(OH)_3] - k_a^{Al(OH)_3}([Al^{3+}][OH^-]^3)^{\lambda_1} \quad (51)$$

$$r_2 = k_d^{CaSO_4.2H_2O}[CaSO_4.2H_2O] - k_a^{CaSO_4.2H_2O}([Ca^{2+}][SO_4^{2-}][OH^-]^2)^{\lambda_2} \quad (52)$$

$$r_3 = k_d^{K_{0.6}Mg_{0.25}Al_{2.3}Si_{3.5}O_{10}(OH)_2}[K_{0.6}Mg_{0.25}Al_{2.3}Si_{3.5}O_{10}(OH)_2] - k_a^{K_{0.6}Mg_{0.25}Al_{2.3}Si_{3.5}O_{10}(OH)_2}([K^+]^2[Mg^{2+}][H^+]^2[Al(OH)_4^-]^2[H_3SiO_4^-]^2)^{\lambda_3} \quad (53)$$

$$r_4 = k_d^{Fe(OH)_3}[Fe(OH)_3] - k_a^{Fe(OH)_3}([Fe^{3+}][OH^-]^3)^{\lambda_4} \quad (54)$$

$$r_5 = k_d^{CaCO_3}[CaCO_3] - k_a^{CaCO_3}([Ca^{2+}][CO_3^{2-}])^{\lambda_5} \quad (55)$$

$$r_6 = k_d^{H_4SiO_4}[H_4SiO_4] - k_a^{H_4SiO_4}([H^+]^2[SiO_2]^2)^{\lambda_6} \quad (56)$$

The model parameters are given in Table 10. The boundary conditions, initial conditions, reaction rates and diffusion coefficients are given in Table 11. PRS2 was chosen to model this example since the diffusion coefficient range is greater than the range of applicability of both PRS0 and PRS1. H^+, Al^{3+} and K^+ were chosen as indicator species.

Table 10 – Model parameters

Parameter	Value
n	0.3
$\gamma_c\ (kg/m^2s)$	$1x10^{-4}$
$p_c^0\ (kN/m^2)$	$1.34x10^3$

Table 11 – BCs, ICs and diffusion coefficients of chemical species

Species	Initial Conc. (kg/kg)	Boundary Conc. A (kg/kg)	Boundary Conc. B (kg/kg)	D^{mol} $(10^{-9}m^2/s)$	Eq.	k_a (10^{-7})	k_d (10^{-8})	λ
H^+	0.000028	0.00005	0.00010	9.311	r_1	2.6	29.6	0.61
Ca^{2+}	0.0003164	0.00048	0.00096	0.792	r_2	0.6	8.67	0.2
Mg^{2+}	0.0010230	0.001944	0.003888	0.706	r_3	1.4	9.0	0.07
HCO_3^-	0.00061	0.000030	0.000060	1.185	r_4	2.8	2.0	0.11
Al^{3+}	0.000837	0.00135	0.00270	0.541	r_5	2.1	6.0	0.43
SO_4^2	0.016896	0.024	0.048	1.065	r_6	0.425	74.0	0.35
Fe^{3+}	0.0019920	0.00279	0.00558	0.604				
K^+	0.0000612	0.000078	0.000156	1.957				
Cl^-	0.0010295	0.001775	0.00355	2.032				
Na^+	0.0018515	0.000345	0.000690	1.334				
SiO_2	0.015	-	-	-				

The dissolved concentration profiles as predicted by the SIS can be seen in Figure 11 for two example species. The dissolved and precipitated mass concentration profiles as predicted by the full model are given in Figure 12 for selected species. An example of the transient behaviour is provided in Figure 13.

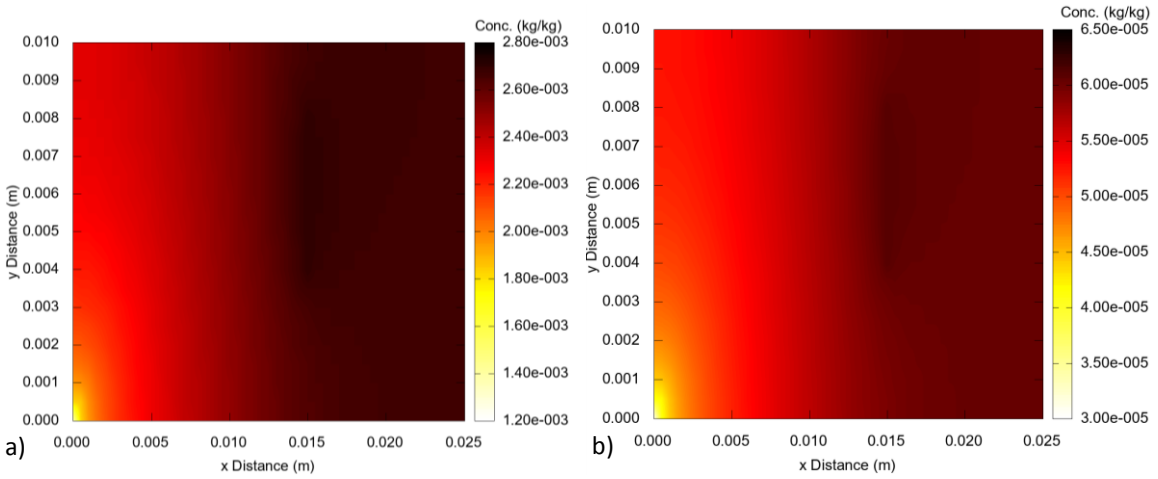

Figure 11 – Dissolved concentrations predicted by the SIS for a) Al^{3+} and b) HCO_3^{2-}

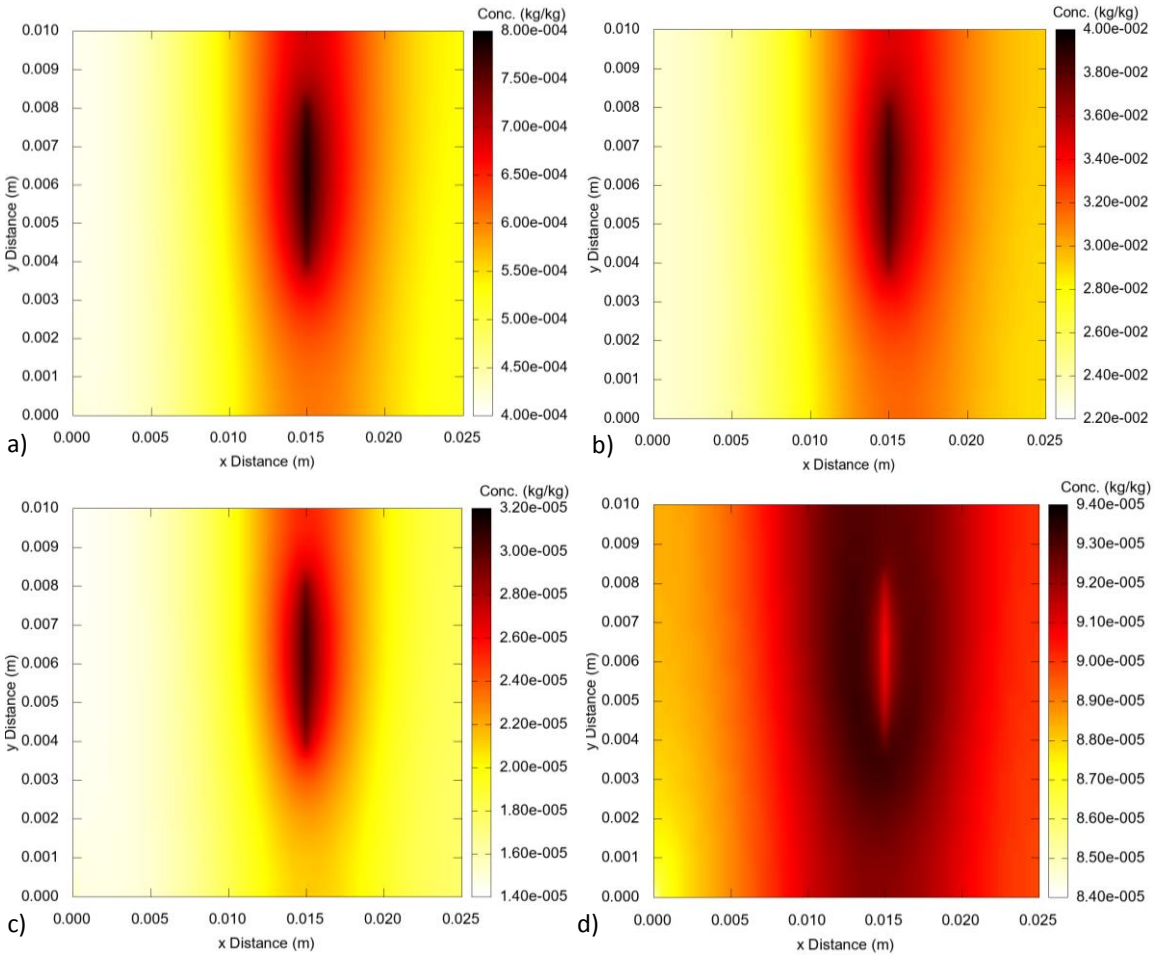

Figure 12 – Dissolved and precipitated mass concentration profiles as predicted by the full model for a) Ca^{+}, b) SO_4^{2-}, c) $Al(OH)_3$ and d) $CaCO_3$ at t=24 hrs

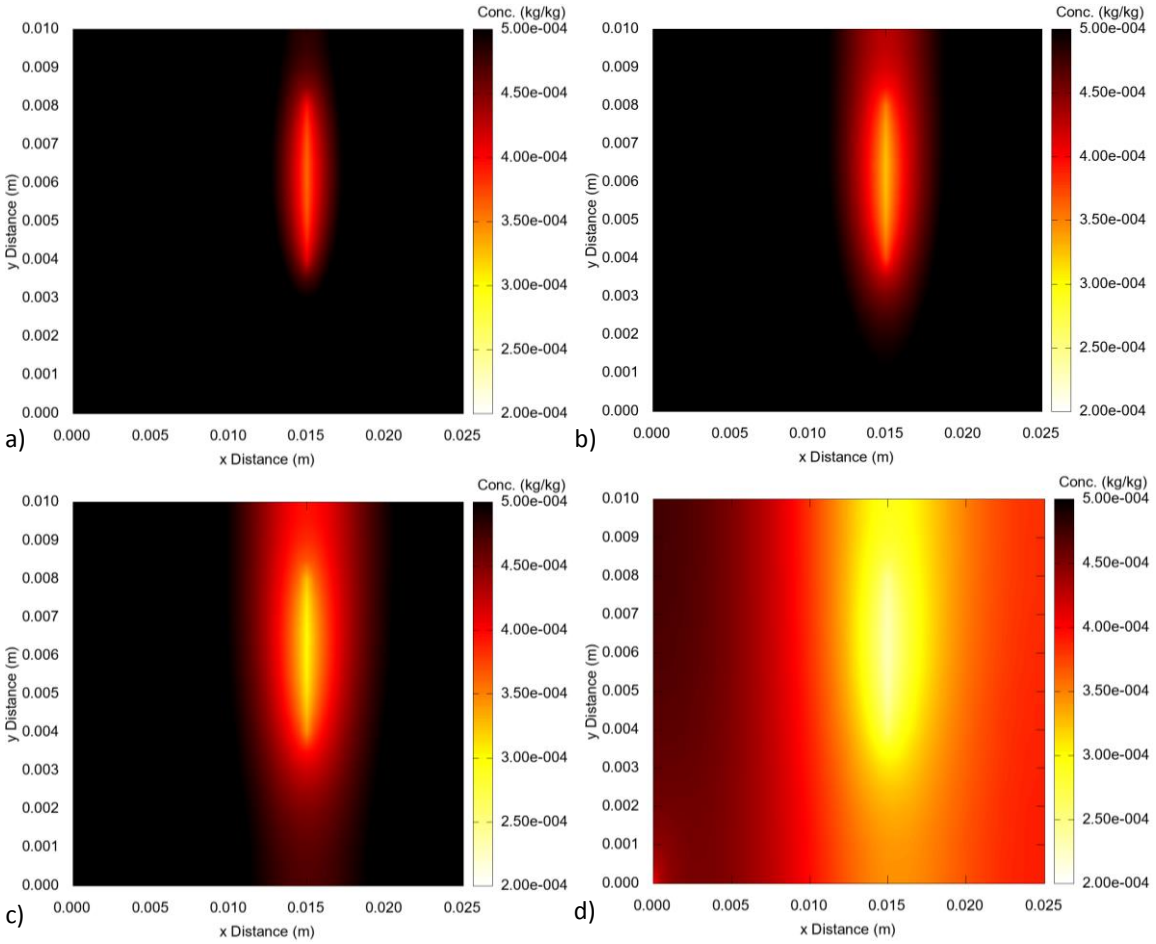

Figure 13 – HCO_3 concentration after a) 2.5 hrs, b) 5 hrs, c) 7.5 hrs and d) 24 hrs

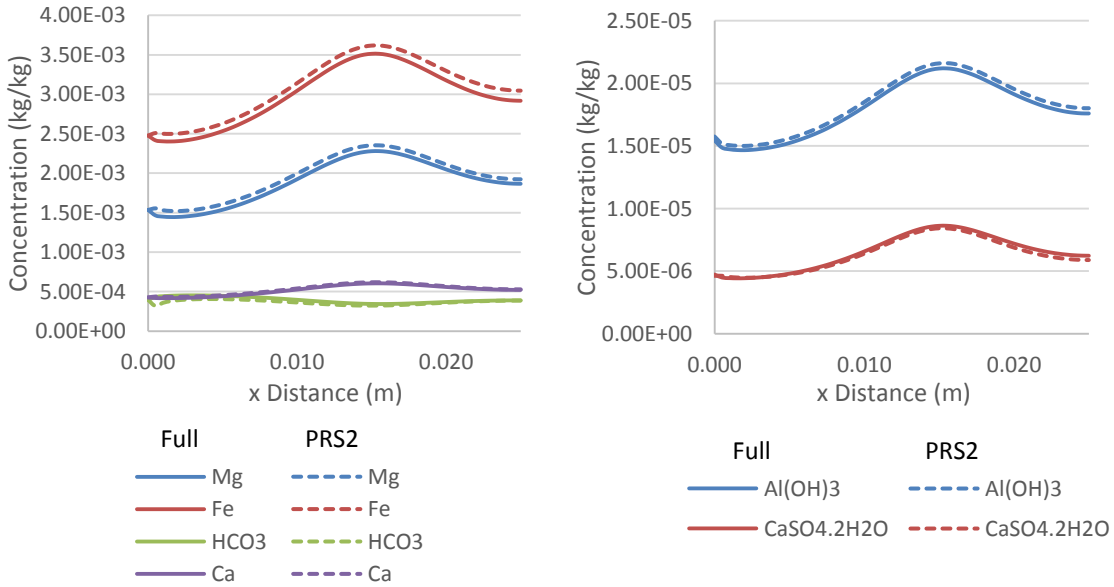

Figure 14 – Longitudinal profiles taken along the x-axis as predicted by the full model and PRS2 at t=24 hrs

It can be seen from the profiles presented in Figure 14 that for this example both the dissolved concentration profiles and the precipitated solids were accurately predicted by the PRS. Figure 14 shows the profiles of a group of species that include species whose diffusion coefficient is furthest

away from an indicator. The results shown are typical of the results of all considered species. The average relative mass balance error in this analysis is 2.77 %. The CPU times using the full model and PRS2 were 8710 s and 1543 s respectively.

7.4 Advection Dominant – PRS1 and PRS2

The final example is based on an advection dominant problem reported by Baroghel-Bouny et al.[35] The problem set up is the same as the diffusion case; however, in this test the sample was first dried at a RH of 4 %, giving a uniform initial moisture content of $S_w=0.09$. The problem has been extended beyond that considered by Baroghel-Bouny et al.[35] with the inclusion of species Ca^{2+} and SO_4^{2-}, and the chemical reaction considered has been changed to the formation of $NaCl$ given by the non-equilibrium Freundlich isotherm:

$$\partial_t(S_p) = -\frac{(S_p - \mu([Na^+][Cl^-])^\lambda)}{\tau} \tag{55}$$

Table 12 – Model parameters

Parameter	Value	Species	Initial Conc. (kg/kg)	Boundary Conc. (kg/kg)	D^{mol} $(10^{-9}m^2/s)$
n	0.13	Na^+	0.003312	0.013524	1.33
μ	0.3	OH^-	0.012274	0.000000	5.3
λ	0.61	K^+	0.024980	0.000000	1.96
τ (s)	72000	Cl^-	0.000000	0.038624	2.1
K_{in} (m^2)	$10\text{x}10^{-21}$	Ca^{2+}	0.000000	0.010000	0.79
p_C^0 (kN/m^2)	$233.6\text{x}10^3$	SO_4^{2-}	0.003000	0.000000	1.07
p_C^b (kN/m^2)	$1.34\text{x}10^3$				

The time period considered was 3 hours and the time step chosen was $\Delta t=0.9\,s$, giving a total number of time steps of 12,000. The finite element mesh and problem geometry were kept the same as for the diffusion case. The model parameters, boundary conditions and diffusion coefficients of the chemical species are given in Table 12. PRS1 and PRS2 were chosen to model this example, with OH^-, Ca^{2+} and Cl^- as indicator species.

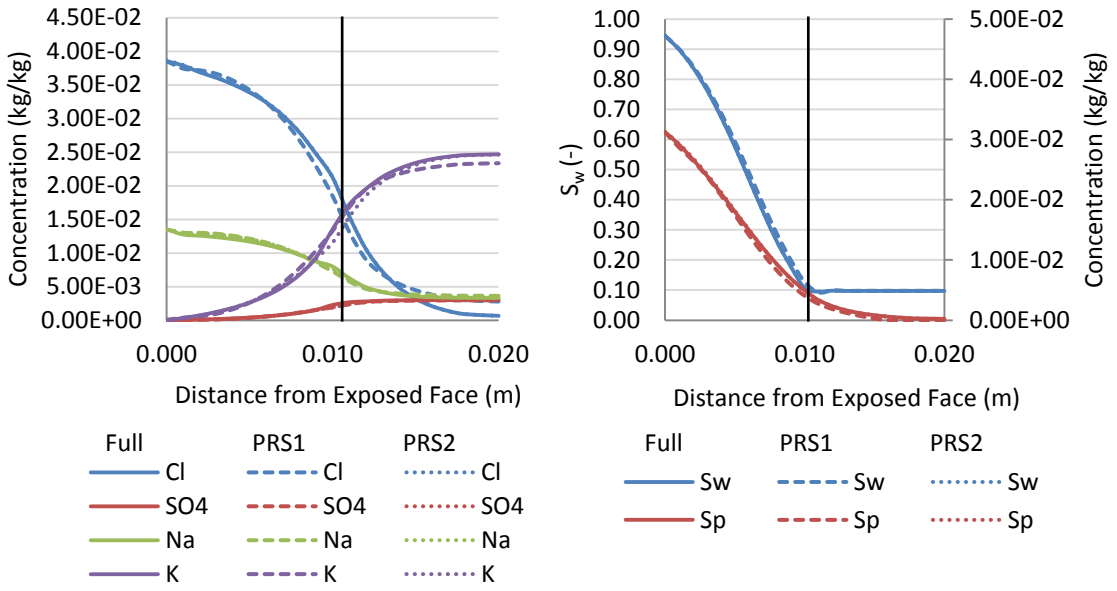

Figure 15 – Concentration, sorbed mass and saturation profiles as predicted by the full model, PRS1 and PRS2 at t=3 hrs (where the black line indicates the position of the wetting front)

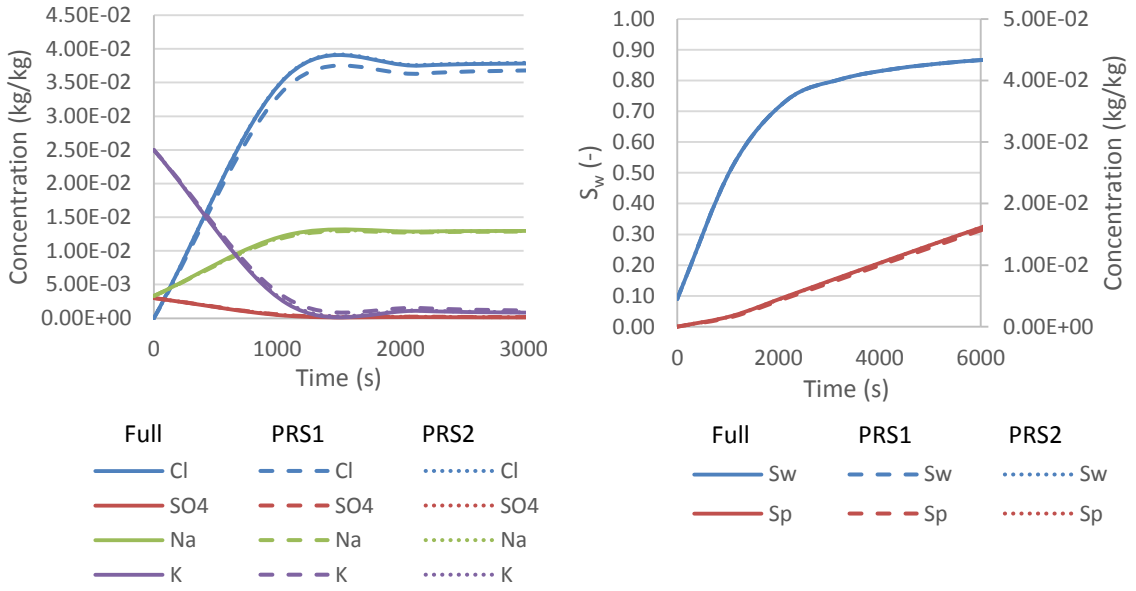

Figure 16 – Transient concentration, sorbed mass and saturation profiles as predicted by the full model, PRS1 and PRS2 at x=1 mm

The concentration, sorbed mass and saturation profiles as predicted by the full model and both PRS1 and PRS2 can be seen in Figure 15; whilst transient profiles corresponding to a point 1 mm from the exposed face are given in Figure 16. The results of the PRS simulations are a good match to those of the full model, with the biggest differences being seen in the Cl^- and K^+ profiles for PRS1. The average relative mass balance error in this analysis is 2.24 % for PRS1 and 1.23 % for PRS2. The CPU time using the full model, PRS1 and PRS2 were 146 s, 83 s and 103 s respectively.

8 Computational Cost

The purpose of the reduction schemes is to reduce the computational cost of solving reactive chemical transport problems. In the above examples, the computational time for solving the problems with PRSs was substantially less than those of the associated full solutions. In order to quantify the reduction in computational cost, CPU times from each of the example problems presented in Sections 6 and 7 using the PRS scheme are compared with those from a full solution. This analysis was performed on a PC with an Intel Core i7-7700HQ @2.80 GHz and 15.9 GB useable RAM. The CPU time of the time step loop was measured for a number of runs and an average taken. The results for each of the problems considered are given in Table 13 and Table 14.

It can be seen from the table that the PRS achieves significant reductions in computational times for the example problems, with reductions being up to 82 % CPU time. The smallest reduction is 29 % for the advection dominant case (where the highly nonlinear moisture transport is responsible for the bulk of the computational cost). It can be seen from Table 14 that the implementation of the reduction scheme does not increase the number of Newton iterations required per time step. Table 14 also shows that the reduction in computational cost achieved by the scheme is a result of reducing the size of the nonlinear system through the reduction of the number of coupled nonlinear PDEs to be solved, as opposed to reducing the nonlinearity of the PDEs or improving the convergence of the Newton-Raphson procedure. The nature of the predictor-corrector approach (eqs. 40 & 41) makes this part of the model readily parallelisable, and, in addition to this, the model is compatible with domain decomposition methods, both of which would reduce the computational cost further.

Finally, it is noted that the reduction in total solution times gained from using the proposed PRS may depend on the moisture transport model employed and whether or not temperature is included as a primary variable. In the present case, the authors considered isothermal problems and have used a single degree of freedom (P_c) to simulate moisture flow, whereas Gawin et al.[32] employed two degrees of freedom in their moisture transport model. The authors expect that the reduction gained, relative to a full model solution, from reducing the number of chemical species that are primary variables would be different if a temperature dependent two-variable moisture model had been used. However, we believe that the use of the PRS will always result in a substantial reduction in CPU time (for any practical engineering problem) when the number of primary chemical species is reduced significantly.

Table 13 – Normalised CPU times and percentage reduction for example problems

Example Problem	Full Model Time (-)	PRS Time (-)			Reduction (%)		
		0	1	2	0	1	2
4 Ion	1	0.616	-	-	38.37	-	-
6 Ion	1	-	0.485	-	-	51.55	-
6 Ion Adv.	1	-	0.571	0.709	-	42.93	29.14
10 Ion	1	-	-	0.177	-	-	82.28
16 Ion*	1	0.226	0.280	0.461	77.39	71.97	53.92

*times given relate to the PRS applied over the applicable ranges and the corresponding full model time

Table 14 – Average Newton iterations for example problems

Example Problem	Full Model Average Iterations (-)	PRS Average Iterations (-)		
		0	**1**	**2**
4 Ion	2	2	-	-
6 Ion	2	-	2	-
6 Ion Adv.	2	-	2	2
10 Ion	2	-	-	2
16 Ion	2	2	2	2

9 Conclusions

The coupled computational model described in this paper is capable of simulating moisture and chemical transport in porous media, as demonstrated in a validation exercise using experimental data from Francy.[35,43]

The computational cost of large-scale multi-species chemical transport problems can become prohibitively expensive and therefore efficient computational procedures and/or problem reduction schemes are required to solve such problems within reasonable times.

The approach of undertaking full solutions for a limited number of chemical (indicator) species and interpolating the response of the other (non-indicator) species provides a direct and effective method for reducing the computational size of multi-species chemical transport problems.

The new predictor-corrector Problem Reduction Scheme (PRS), based on a Lagrangian interpolation and a mass balance correction, is able to solve multi-species coupled chemical transport problems with good accuracy and efficiency, with errors in chemical concentration and mass being within 1 % and 4 % respectively of those from a full solution. The accuracy of the PRS depends on the order of the scheme, with higher order schemes being applicable to problems that have larger ranges of diffusion coefficients. The range of applicability of zero, first and second order schemes (with 1,2 and 3 indicator species respectively), in terms of a reference (lower) diffusion constant D, are D to $1.9D$, D to $6D$ and D to $16D$ respectively with an accuracy of 1 % (or 3 % for PRS0).

The reduction in computational cost of an example 10-ion transport problem using the PRS is 82 % relative to the corresponding cost of a full solution.

Overall, the new numerical procedure described in this paper has the potential to offer significant reductions in computational demand for highly coupled multi-species reactive transport models. Furthermore, the particular nature of the PRS algorithm makes it suitable for parallelisation, and the scheme is compatible with domain decomposition methods. This implies that the proposed PRS is capable of overcoming existing barriers to the exploitation of supercomputing facilities in the solution of such coupled problems.

Acknowledgements

The primary financial support for this work was from the EPSRC Grant EP/P02081X/1 "Resilient materials for life (RM4L)", which we gratefully acknowledge.

We would also like to acknowledge support from NERC Grant NE/L013908/1 ''In situ recovery of resources from waste repositories''.

Information on the data underpinning the results presented here, including how to access them, can be found in the Cardiff University data catalogue at (http://doi.org/10.17035/d.2019.0079832549).

Appendix A

Constitutive Relation	Expression	Values
Kelvin's law[22]	$P_c = \frac{-\rho_w RT}{M_w} \ln\left(\frac{P_v}{P_{vs}}\right)$	$M_w = 18\ kg/kmol$ $R = 8314.5\ J/K\ kmol$
Dalton's law[22]	$P_g = P_{da} + P_v$	-
Antoine's law[22]	$\rho_{vs} = b_1 \cdot 10^{b_2 - \frac{b_3}{b_4 + T - b_5}}$	$b_1 = 133.32, b_2 = 8.07,$ $b_3 = 1730.63, b_4 = 233.43$ $b_5 = 273$
Moisture retention[22,46]	$S_w = \left(\left(\frac{P_C}{a}\right)^{\frac{1}{1-m}} + 1\right)^{-m}$	$a = 1.867 \times 10^7\ Pa$ $m = 0.44$

References

1. Bear J, Bachmat Y. *Introduction to modelling of transport phenomena in porous media*. The Netherlands: Kluwer Academic Publishers; 1990.

2. Yeh G, Tripathi VS. A Model for Simulating Transport of Reactive Multispecies Components: Model Development and Demonstration. *Water Resources Research* 1991;27(12):3075–3094.

3. Engesgaard P, Kipp KL. A geochemical transport model for redox-controlled movement of mineral fronts in groundwater flow systems: A case of nitrate removal by oxidation of pyrite. *Water Resources Research* 1992; 28(10):2829–2843. doi:10.1029/92WR01264.

4. Walter AL, Frind EO, Blowes DW, Ptacek CJ, Molson JW. Modeling of multicomponent reactive transport in groundwater. 1.Model development and evaluation. *Water Resources Research* 1994; 30(1):3137–3148.

5. Appelo CAJ, Rolle M. PHT3D: A reactive multicomponent transport model for saturated porous media. *Ground Water* 2010; 48(5):627–632. doi:10.1111/j.1745-6584.2010.00732.x.

6. Parkhurst DL, Wissmeier L. PhreeqcRM: A reaction module for transport simulators based on the geochemical model PHREEQC. *Advances in Water Resources* 2015; 83:176–189. doi:10.1016/j.advwatres.2015.06.001.

7. Gens A, do N. Guimarães L, Olivella S, Sánchez M. Analysis of the THMC Behaviour of Compacted Swelling Clay for Radioactive Waste Isolation. In: Stephanson O, ed. *Coupled Thermo-*

Hydro-Mechanical-Chemical Processes in Geo-Systems Fundamentals, Modelling, Experiments and Applications, vol 2. Elsevier; 2004:317–322.

8. Cleall PJ, Seetharam SC, Thomas HR. Inclusion of Some Aspects of Chemical Behavior of Unsaturated Soil in Thermo/Hydro/Chemical/Mechanical Models. I: Model Development. *Journal of Engineering Mechanics* 2007; 133(3):348–356. doi:10.1061/(ASCE)0733-9399(2007)133:3(348).

9. Cleall PJ, Seetharam SC, Thomas HR. Inclusion of Some Aspects of Chemical Behavior of Unsaturated Soil in Thermo/Hydro/Chemical/Mechanical Models. II: Application and Transport of Soluble Salts in Compacted Bentonite. *Journal of Engineering Mechanics* 2007; 133(3):348–356. doi:10.1061/(ASCE)0733-9399(2007)133:3(348).

10. Thomas HR, Sedighi M, Vardon PJ. Diffusive Reactive Transport of Multicomponent Chemicals Under Coupled Thermal, Hydraulic, Chemical and Mechanical Conditions. *Geotechnical and Geological Engineering* 2012; 30(4):841–857. doi:10.1007/s10706-012-9502-9.

11. Sedighi M, Thomas HR, Vardon PJ. Reactive transport of chemicals in unsaturated soils: numerical model develomment and verification. *Canadian Geotechnical Journal* 2015; 52(June 2015):162–172. doi:10.1016/B978-0-12-385920-4.00013-8.

12. Zhu C, Fang H, Anderson G, Burden D. Reactive mass transport modeling of natural attenuation of an acid plume at a uranium mill tailings site. *Abstracts with Programs - Geological Society of America* 1999; 31:69–70. doi:10.1016/S0169-7722(01)00154-1.

13. Banwart SA, Malmström ME. Hydrochemical modelling for preliminary assessment of minewater pollution. *Journal of Geochemical Exploration* 2001; 74(1–3):73–97. doi:10.1016/S0375-6742(01)00176-5.

14. Bertocchi AF, Ghiani M, Peretti R, Zucca A. Red mud and fly ash for remediation of mine sites contaminated with As, Cd, Cu, Pb and Zn. *Journal of Hazardous Materials* 2006; 134(1–3):112–119. doi:10.1016/j.jhazmat.2005.10.043.

15. Thomas MDA, Bamforth PB. Modelling chloride diffusion in concrete effect of fly ash and slag. *Cement and Concrete Research* 1999; 29(4):487–495. doi:10.1016/S0008-8846(98)00192-6.

16. Song HW, Lee CH, Ann KY. Factors influencing chloride transport in concrete structures exposed to marine environments. *Cement and Concrete Composites* 2008; 30(2):113–121. doi:10.1016/j.cemconcomp.2007.09.005.

17. Baroghel-Bouny V, Nguyen TQ, Dangla P. Assessment and prediction of RC structure service life by means of durability indicators and physical/chemical models. *Cement and Concrete Composites* 2009; 31(8):522–534. doi:10.1016/j.cemconcomp.2009.01.009.

18. Koniorczyk M, Gawin D. Modelling of salt crystallization in building materials with microstructure - Poromechanical approach. *Construction and Building Materials* 2012; 36:860–873. doi:10.1016/j.conbuildmat.2012.06.035.

19. Kuhl D, Bangert F, Meschke G. Coupled chemo-mechanical deterioration of cementitious materials. Part I: Modeling. *International Journal of Solids and Structures* 2004; 41(1):15–40.

20. Gawin D, Pesavento F, Schrefler BA. Modeling deterioration of cementitious materials exposed to calcium leaching in non-isothermal conditions. *Computer Methods in Applied Mechanics and Engineering* 2009; 198(37–40):3051–3083. doi:10.1016/j.cma.2009.05.005.

21. Aliko-Benítez A, Doblaré M, Sanz-Herrera JA. Chemical-diffusive modelling of the self-healing behavior in concrete. *International Journal of Solids and Structures* 2015; 70:392–402. doi:10.1016/j.ijsolstr.2015.05.011.

22. Chitez AS, Jefferson AD. A coupled thermo-hygro-chemical model for characterising autogenous healing in ordinary cementitious materials. *Cement and Concrete Research* 2016; 88:184–197. doi:10.1016/j.cemconres.2016.07.002.

23. Cleall PJ, Thomas HR, Melhuish TA, Owen DH. Use of parallel computing and visualisation techniques in the simulation of large scale geoenvironmental engineering problems. *Future Generation Computer Systems* 2006; 22(4):460–467.http://www.scopus.com/inward/record.url?eid=2-s2.0-29644438234&partnerID=40&md5=e97d1ecff92867bbe5a7becd7f140a61Accessed.

24. Valocchi AJ, Malmstead M. Accuracy of operator splitting for Advection-Dispersion-Reaction Problems. *Water Resources Research* 1992; 28(5):1471–1476.

25. Yeh GT, Tripathi VS. A critical evaluation of recent developments in hydrogeochemical transport models of reactive mutichemical components. *Water Resources Research* 1989; 25(1):93–108. doi:10.1029/WR025i005p01066.

26. Kräutle S, Knabner P. A reduction scheme for coupled multicomponent transport-reaction problems in porous media: Generalization to problems with heterogeneous equilibrium reactions. *Water Resources Research* 2007; 43(3). doi:10.1029/2005WR004465.

27. Hoffmann J, Kräutle S, Knabner P. A general reduction scheme for reactive transport in porous media. *Computational Geosciences* 2012; 16(4):1081–1099. doi:10.1007/s10596-012-9304-4.

28. Saaltink MW, Carrera J, Ayora C. On the behavior of approaches to simulate reactive transport. *Journal of Contaminant Hydrology* 2001; 48(3–4):213–235. doi:10.1016/S0169-7722(00)00172-8.

29. Friedly JC, Rubin J. Solute transport with multiple equilibrium controlled or kinetically controlled chemical reactions. *Water Resources Research* 1992; 28:1935–1953.

30. Molins S, Carrera J, Ayora C, Saaltink MW. A formulation for decoupling components in reactive transport problems. *Water Resources Research* 2004; 40(10):1–13. doi:10.1029/2003WR002970.

31. Zhang F, Yeh GT, Parker JC, et al. A reaction-based paradigm to model reactive chemical transport in groundwater with general kinetic and equilibrium reactions. *Journal of Contaminant Hydrology* 2007; 92(1–2):10–32. doi:10.1016/j.jconhyd.2006.11.007.

32. Gawin D, Pesavento F, Schrefler BA. Hygro-thermo-chemo-mechanical modelling of concrete at early ages and beyond. Part I: hydration and hygro-thermal phenomena. *International Journal for Numerical Methods in Engineering* 2006; 67(3):299–331. doi:10.1002/nme.1615.

33. Chitez AS, Jefferson AD. Porosity development in a thermo-hygral finite element model for cementitious materials. *Cement and Concrete Research* 2015; 78:216–233. doi:10.1016/j.cemconres.2015.07.010.

34. Lewis RW, Schrefler BA. *The finite element method in the static and dynamic deformation and consolidation of porous media.* 2nd ed. Great Britian: John Wiley and Sons Inc.; 1998.

35. Baroghel-Bouny V, Thiéry M, Wang X. Modelling of isothermal coupled moisture-ion transport in cementitious materials. *Cement and Concrete Research* 2011; 41(8):828–841. doi:10.1016/j.cemconres.2011.04.001.

36. Song Z, Jiang L, Chu H, Xiong C, Liu R, You L. Modeling of chloride diffusion in concrete immersed in CaCl2 and NaCl solutions with account of multi-phase reactions and ionic interactions. *Construction and Building Materials* 2014; 66:1–9. doi:10.1016/j.conbuildmat.2014.05.026.

37. Lasaga AC, The treatment of multi-component diffusion and ion pairs in diagenetic fluxes. *American Journal of Science* 1979; 279(3):324-346

38. Rubin J, Transport of reacting solutes in porous media: Relation between mathematical nature of problem formulation and chemical nature of reactions. *Water Resour. Res.* 1983; 19(5):1231-1252

39. Scovazzi G, Wheeler A, Mikelić, A, Lee S, Analytical and variational numerical methods for unstable miscible displacement flows in porous media. *Journal of Computational Physics*. 2017; 335:444-496

40. Brooks AN, Hughes TJR, Streamline upwind/Petrov-Galerkin formulations for convection dominated flows with particular emphasis on the incompressible Navier-Stokes equations. *Computer Methods in Applied Mechanics and Engineering*. 1982;32(1-3):199-259

41. Pan L, Wierenga P, Finite element methods for modeling water flow in variably saturated porous media: Numerical oscillation and mass-distributed schemes. *Water Resour. Res.* 1996;32(6):1883-1889

42. Fetter CW, *Contaminant Hydrogeology*, 2nd ed. USA: Prentice-Hall, 1998

43. Francy O. *Modelling of chloride ions ingress in partially water saturated mortars*. (in French). Ph.D. Thesis, Paul Sabatier Univ., Toulouse, France, 1998.

44. McLaughlin B, Peterson J, Ye M, Stabilized reduced order models for the advection-diffusion-reaction equation using operator splitting. *Computers and Mathematics with Applications*. 2016;71(11):2407-2420

45. Luo Z, Li H, Zhou Y, Xie Z, A reduced finite element formulation based on POD method for two-dimensional solute transport problems. *Journal of Mathematical Analysis and Applications*. 2012;385(1):371-383

46. van Genuchten MT. A Closed-form Equation for Predicting the Hydraulic Conductivity of Unsaturated Soils. *Soil Science Society of America Journal* 1980; **44**(5):892-898.